Available online at www.sciencedirect.com
ScienceDirect
Geochimica et Cosmochimica Acta 71 (2007) 4745–4770
Geochimica et Cosmochimica Acta
www.elsevier.com/locate/gca

Iron isotope, major and trace element characterization of early Archean supracrustal rocks from SW Greenland: Protolith identification and metamorphic overprint

Nicolas Dauphas [a,b,*], Mark van Zuilen [c], Vincent Busigny [a,b,1], Aivo Lepland [d], Meenakshi Wadhwa [e], Philip E. Janney [e]

[a] *Origins Laboratory, Department of the Geophysical Sciences and Enrico Fermi Institute, The University of Chicago, 5734 South Ellis Avenue, Chicago, IL 60637, USA*
[b] *The Field Museum, 1400 South Lake Shore Drive, Chicago, IL 60605, USA*
[c] *Equipe Biogéosphère Actuelle et Primitive, Institut de Physique du Globe de Paris, 4 Place Jussieu, 75252 Paris Cedex 05, France*
[d] *Geological Survey of Norway, 7491 Trondheim, Norway*
[e] *School of Earth and Space Exploration, Arizona State University, Box 871404, Tempe, AZ 85287, USA*

Received 15 February 2007; accepted in revised form 16 July 2007; available online 23 August 2007

Abstract

The iron isotope, trace and major element compositions of Eoarchean supracrustal rocks from southern West Greenland (Isua Supracrustal Belt, the islands of Akilia and Innersuartuut) were analyzed in order to identify protoliths and characterize the imprints of metamorphism and metasomatism. Banded iron formations (BIFs) from the Isua Supracrustal Belt (ISB) have trace element characteristics that are consistent with seawater derivation, including high Y/Ho ratios, positive Eu/Eu* anomalies, positive La/La* anomalies, and concave upward REE patterns. These rocks also have heavy Fe isotopic compositions relative to surrounding igneous rocks (~+0.4‰/amu). The most likely interpretation is that this signature was inherited from partial oxidation in a marine setting of Fe emanating from a source similar to modern mid-ocean ridge hydrothermal vents (~−0.15‰/amu).

Banded quartz-rich rocks from the island of Akilia with high Fe/Ti ratios share many similarities with *bona fide* BIFs from Isua (heavy Fe isotopic compositions up to +0.4‰/amu, elevated Y/Ho ratios compared to igneous rocks, sometimes positive Eu/Eu* anomalies) suggesting a chemical sedimentary origin.

Iron-poor metacarbonates from the southwestern part of the ISB have light Fe isotopic compositions (~−0.4‰/amu). This is consistent with derivation of these rocks by fluid flow through surrounding ultramafic rocks and deposition as metasomatic carbonates. Iron-rich metacarbonates from the northwest and northeast parts of the ISB have Fe isotopic compositions (from +0.1 to +0.4‰/amu) and trace element patterns (high Y/Ho ratios, positive Eu/Eu* and La/La* anomalies, and concave upward REE) similar to associated BIFs. The most likely interpretation is that these iron-rich metacarbonates were derived from mobilization of Fe in BIFs by metasomatic fluids.

1. INTRODUCTION

The terrestrial record of supracrustal rocks (i.e., lithologies formed at the top of the crust such as lava flows and sediments) extends to ~3.8 Ga but the quality of this record degrades with the antiquity of the rocks studied (e.g., Moorbath et al., 1973; Nutman et al., 1989, 1997; Schiøtte

* Corresponding author.
E-mail address: dauphas@uchicago.edu (N. Dauphas).
[1] Present address: Laboratoire de Géochimie des Isotopes Stables, Institut de Physique du Globe de Paris et Université Paris 7, 2 Place Jussieu, 75252 Paris Cedex 05, France.

0016-7037/$ - see front matter © 2007 Elsevier Ltd. All rights reserved.
doi:10.1016/j.gca.2007.07.019

et al., 1989; David et al., 2002; Cates and Mojzsis, 2007; Dauphas et al., 2007). The main reason is that ancient rocks were buried in the crust at high pressure and temperature, which modified original structures and mineral assemblages. In addition, interactions with crustal fluids have, in many cases, obliterated chemical and isotopic fingerprints. The numerous controversies that surround the nature of Eoarchean rocks attest to the difficulty of interpreting the message carried by these samples. The isotopic compositions of S (Mojzsis et al., 2003; Whitehouse et al., 2005), Si (André et al., 2006), and Fe (Dauphas et al., 2004a) have recently been shown to be good tracers of seawater derivation and can thus be used to elucidate some of these controversies. In the present study, we have targeted two types of samples from SW Greenland for which contradictory interpretations have been proposed,

(i) The carbonates found in the Isua Supracrustal Belt (ISB) were initially interpreted to represent chemical sediments that had partially reacted at contact with host lithologies during burial and associated high P–T metamorphism (Schidlowski et al., 1979; Appel, 1980, 1983; Nutman et al., 1984; Dymek and Klein, 1988; Shimizu et al., 1990; Mojzsis et al., 1996; Bolhar et al., 2004). An alternative school of thought is that carbonate rocks found in the ISB are metasomatic in origin (Rose et al., 1996; Rosing et al., 1996; Lepland et al., 2002; van Zuilen et al., 2005). In that scenario, calc-silicate rocks surrounding ultramafic bodies were formed by desilicification and carbonation of country rocks by fluids flowing out of the ultramafic units.

(ii) A >3.7–3.8 Ga layered quartz-pyroxene (Qtz-Px) formation found on the island of Akilia (SW Greenland) has been interpreted by some as a highly metamorphosed chemical sedimentary formation (McGregor and Mason, 1977; Mojzsis et al., 1996; Nutman et al., 1997; Friend et al., 2002; Mojzsis and Harrison, 2002; Palin, 2002; Dauphas et al., 2004a; Manning et al., 2006). Others prefer a metasomatic interpretation whereby mafic and ultramafic protoliths were modified by quartz addition and tectonic reworking (Fedo and Whitehouse, 2002a,b,c; Bolhar et al., 2004; André et al., 2006; Fedo et al., 2006).

Identifying possible chemical sediments in Eoarchean terranes is crucial because some of these formations have been proposed to host Earth's earliest remnants of life and they represent the only direct witnesses of the composition of the atmosphere/ocean system at that time. Here, we examine the Fe isotope, major and trace element compositions of metacarbonates from Isua and banded quartz-pyroxene rocks from the island of Akilia to distinguish between primary depositional features of chemical sediments and metasomatic/metamorphic modifications. In Section 2, we briefly review the Eoarchean geology of SW Greenland. In Section 3, the methods used in this study are explained. In Section 4, the results are presented. In Section 5, we discuss the implications of these results for the formation of the metacarbonates found in Isua and the Qtz-Px banded rocks from the island of Akilia. In this section, we also discuss calibration of magnetite-carbonate and magnetite-pyroxene iron isotope geothermometers.

2. REGIONAL GEOLOGY AND SAMPLE DESCRIPTION

2.1. The Isua Supracrustal Belt

2.1.1. Major geological units

The ISB is part of the 3.8 Ga Itsaq Gneiss Complex in southern West Greenland, and represents one of the earliest records of a hydrosphere on Earth. It consists of an assemblage of metavolcanic and metasedimentary rocks with a complex metamorphic history. Multiple amphibolite-facies metamorphic events ($T = 500$–600 °C, $P < 5.5$ kbar, Boak and Dymek, 1982; Rollinson, 2003) were responsible for ductile deformation, shearing, mylonite formation, and strong metasomatic alteration. Extensive mapping efforts (Nutman et al., 1984, 1996, 1997, 2000, 2002a; Nutman, 1986; Rosing et al., 1996; Appel et al., 1998; Komiya et al., 1999; Fedo, 2000; Myers and Crowley, 2000; Fedo et al., 2001; Myers, 2001) have shown that the lithological diversity in the ISB is the result of metasomatic fluid–rock reactions of a small number of protoliths. Due to this strong metasomatic overprint, there still is a debate over the protolith recognition of certain rocks and the associated depositional environment they represent. The different rock types that are generally recognized in the ISB, include (Fig. 1):

(1) Garbenschiefer amphibolites representing a volcano-sedimentary pile. In places pillow lava structures have been preserved (Komiya et al., 1999) suggesting that the majority of these rocks consist of strongly altered metabasalts. Several sedimentary units have been recognized within this pile including graded beds with Bouma-sequence structures (Rosing et al., 1996; Rosing, 1999).
(2) Less common highly metasomatized amphibolites representing altered gabbros.
(3) Magnetite-quartz banded rocks representing sequences of cherts and banded iron formations (BIFs). These rocks are interpreted as marine chemical sediments.
(4) Quartzo-feldspathic schists and gneisses which have been interpreted as felsic volcanic and volcanoclastic deposits (e.g. Nutman et al., 2002a). In some places, however, these rocks show gradation into discordant sheets of tonalitic gneisses, and have therefore been interpreted as metasomatized tonalitic intrusives (Rosing et al., 1996).
(5) Ultramafic bodies representing metamorphosed dunitic–peridotitic sill-like intrusions.
(6) Carbonate-rich rocks representing a wide variety of rocks from calc-silicates to pure metacarbonates. These rocks were initially interpreted as a sedimentary pile that had formed in a predominantly shallow marine environment (Dimroth, 1982). In many

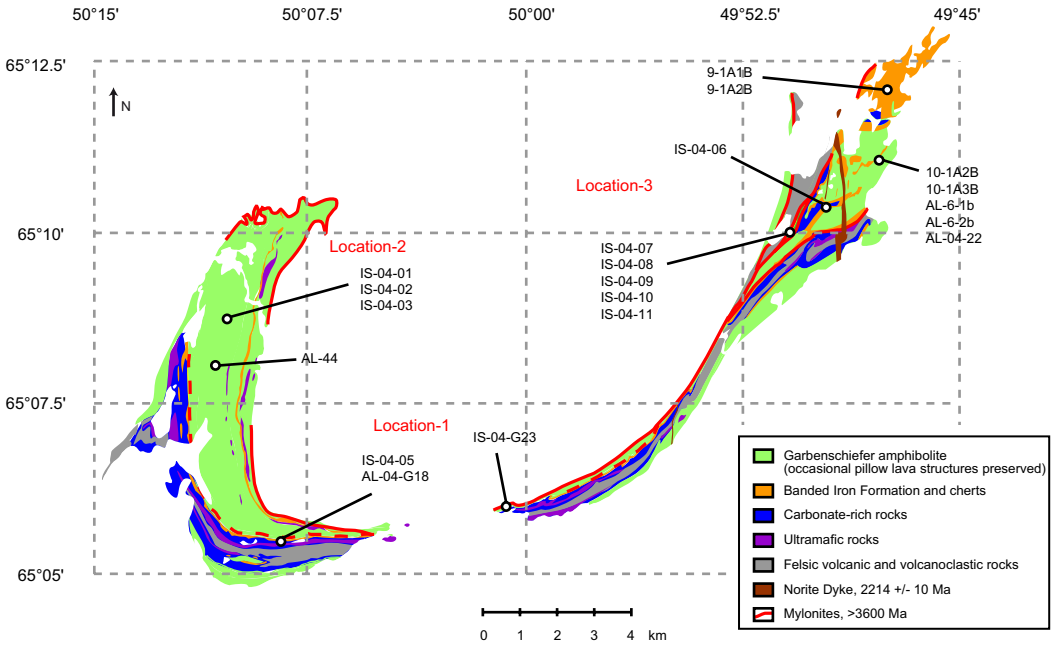

Fig. 1. Geologic map of the ISB, southern West Greenland (this geologic representation is a generalization based on several publications, the most important being Nutman, 1986; Nutman et al., 1996, 1997, 2000, 2002a; Rosing et al., 1996; Appel et al., 1998; Myers, 2001). Several metavolcanic and metasedimentary formations are recognized, that are intruded by mafic and ultramafic rocks. The Garbenschiefer amphibolite unit is an assemblage of volcano-sedimentary rocks, altered pillow-lava basalts, and highly altered gabbros. Recently, a sheeted dike complex has been recognized in this unit as well (Furnes et al., 2007). The carbonate-rich rocks represent an assemblage of calc-silicates and metacarbonates. Samples of undisputed banded iron formations occur in a zone of relatively low strain, in the northeastern part of the belt. Samples of metacarbonate rocks have been obtained from three locations; the southwestern part of the belt (Location 1) that is dominated by ultramafic intrusions, the northwestern part of the belt (Location 2) that is dominated by amphibolite schists of the Garbenschiefer unit, and the northeastern part of the belt (Location 3) that occurs in a major shear zone (shown as a mylonite) directly south of the major outcrops of banded iron formations.

places, however, calc-silicates and metacarbonates were found associated with ultramafic bodies, or in cross-cutting relationship with other host rocks.

Rose et al. (1996) and Rosing et al. (1996) proposed a metasomatic model for the emplacement of carbonates in the ISB by high-T fluid migration through ultramafic rocks. This model was motivated from field observations showing that (i) metacarbonate rocks are associated with ultramafic rocks, and often form envelopes around these intrusives; (ii) contacts between metacarbonates and other metasedimentary or metavolcanic units are metasomatic (e.g., carbonate interfingering with host rock lithology, fluid advection along fractures); and (iii) there is a continuum between metacarbonates and moderately carbonated host lithologies. Rose et al. (1996) devised a numerical simulation of metasomatism in the ISB whereby fluids flow through an ultramafic unit and react with country rocks at the downstream contact to form carbonated mineral assemblages similar to those found in the ISB. The field evidence for this model is best represented in the southwestern part of the ISB, where many metacarbonates occur as 1–10 m wide rims that follow the outline of elongate ultramafic bodies (e.g., Fig. 4a–d in Rose et al., 1996). As noted by Rose et al. (1996), metacarbonates are not invariably found in contact with ultramafic rocks. Fluids may migrate for some distance along faults and fractures before reacting with country rock to form metacarbonate zones.

2.1.2. Sample descriptions

Undisputed metasedimentary units such as BIFs, metacherts, and graded beds, have a limited distribution in the ISB. The largest outcrops of metasediments occur in the north-eastern part of the ISB (Fig. 1), within a zone of relatively low strain (Appel et al., 1998; Fedo, 2000). Sample IS-04-06 represents a small outcrop of very well preserved BIF, which exhibits fine (mm-scale) quartz-magnetite banding. This rock also contains considerable amounts of calcite and tremolite/actinolite. Samples 9-1A1B and 9-1A2B represent the largest outcrop of BIF in the extreme northeastern part of the ISB. This rock also consists predominantly of quartz and magnetite bands, with minor chlorite and amphiboles. Slightly to the south of this, pyrite-rich quartz-magnetite BIF (samples 10-1A2B, 10-1A3B, and AL6-2b) and pyrite-rich magnetite-free chert (AL-04-G22) occur. The pyrite in these samples has clearly been remobilized as it typically occurs in veinlets.

All other samples represent carbonate-rich rocks of uncertain origin. Evidence for pervasive metasomatic carbonation throughout the ISB has complicated their interpretation. Studied samples were collected from three

general areas (Fig. 1); location 1 in the south (IS-04-05, AL-04-G18, AL-04-G23), location 2 in the northwest (IS-04-01 to IS-04-03), and location 3 in the northeast (IS-04-07 to IS-04-11). Samples of location 1 are directly surrounded by ultramafic intrusions. Sample IS-04-05 consists predominantly of calcite and dolomite (Fig. 2), with smaller amounts of tremolite/actinolite. At the location of sample IS-04-05 a replacive metasomatic character of carbonates is observed (Fig. 3a–c), that is similar to the earlier descriptions of Rose et al. (1996). The samples of location 2 (Fig. 3d–f) represent elongated trains of carbonate lenses that consist predominantly of Mg-siderite (Fig. 2), with smaller amounts of tremolite/actinolite, chlorite, and Fe-oxyhydroxide. Sample IS-04-01 also contains magnetite. Samples of location 3 occur in a shear zone in the northeastern part of the belt. These rocks appear as dark elongated lenses and veins in a garnet-amphibolite schist host rock. They consist predominantly of Mg-siderite (Fig. 2), magnetite, grunerite/cummingtonite, chlorite, and garnet. Graphite and apatite are conspicuous minor phases in all of these samples. Several earlier studies have recognized these rocks as metasomatic carbonate deposits (Fig. 3g

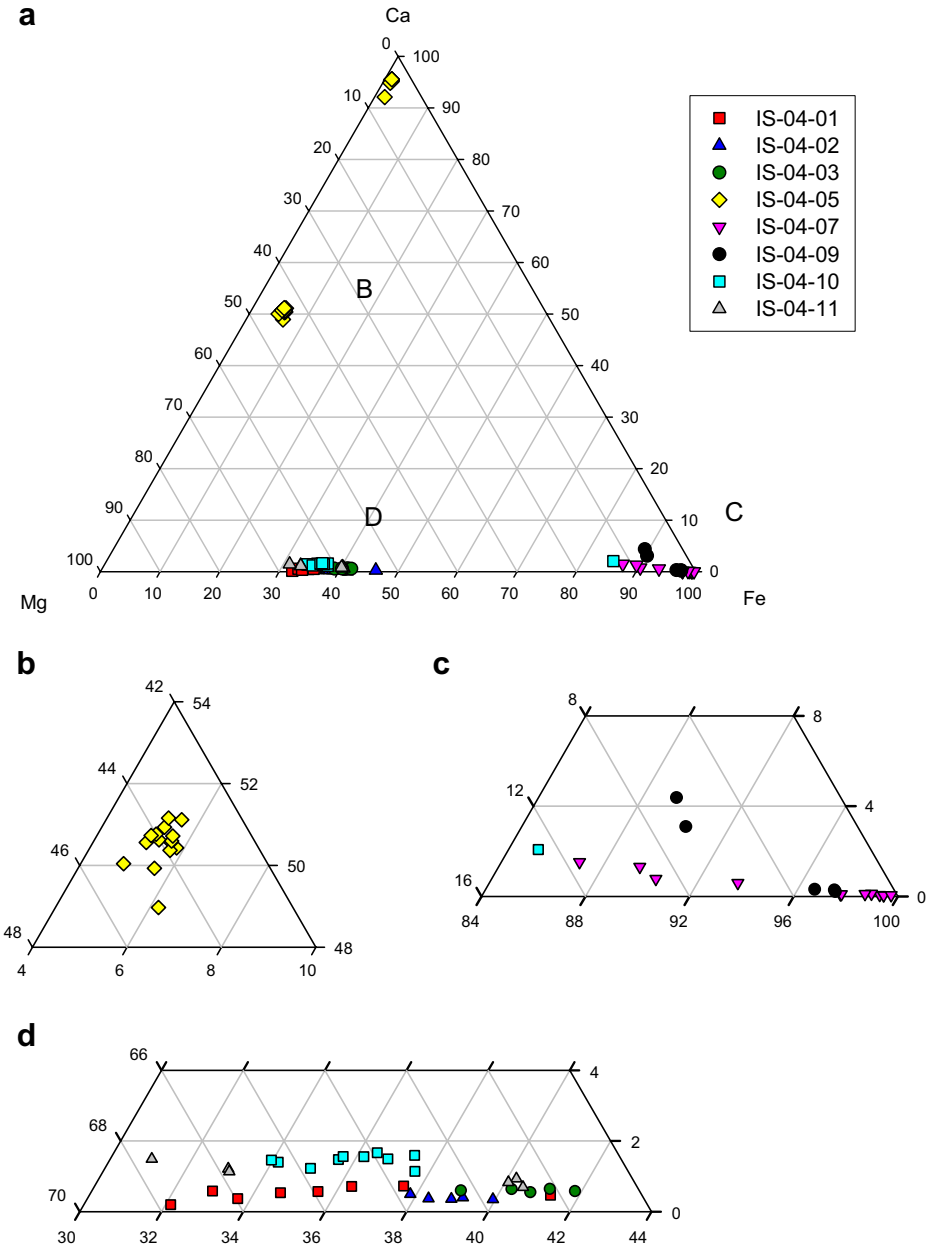

Fig. 2. Ca–Mg–Fe ternary plot showing the cation composition of carbonate fractions in metacarbonate samples from the ISB (a). Cation concentrations were measured by electron microprobe, and are calculated in mol g^{-1}. Carbonate compositions are restricted to four different types: calcite, dolomite, Mg-siderite, and pure siderite. Mg-siderite and pure siderite also contain minor Mn. Areas in (a) indicated as "B", "C", and "D" are shown on expanded scale in (b), (c), and (d).

Fig. 3. Field appearance of metacarbonate samples from the ISB. Location 1 in the southwestern part of the ISB shows metacarbonates closely associated with ultramafic bodies, that have pervasively infiltrated the host rock (a–c). Location 2 in the northwestern part shows metacarbonate lenses that infiltrated an amphibolite-schist host rock (d–f). Location 3 in the northeastern part shows graphite–magnetite-rich metacarbonate lenses within a garnet–chlorite–amphibolite–schist host rock. These lenses occur in a general shear zone that runs from the northeast to the southwest (g–i).

and h). It was further recognized that part of the Mg-siderite fraction in these rocks has thermally decomposed to magnetite and graphite during one or more metamorphic events (Lepland et al., 2002; van Zuilen et al., 2002, 2003). Mineral modes of the metacarbonates are given in Table 1.

2.2. The Akilia association

In the southwestern extension of the island of Akilia, a small enclave of supracrustal rocks has been subject to strong deformation and local partial melting at amphibolite to granulite facies metamorphism (Fig. 4). The dominant lithology of this enclave consists of mafic amphibolite gneisses and ultramafics. Within these igneous surroundings a 5-m wide outcrop of quartz-pyroxene rock is present. It has been interpreted either as a strongly metamorphosed and deformed BIF (Mojzsis et al., 1996; Nutman et al., 1997) or as a metasomatized ultramafic rock (Fedo and Whitehouse, 2002a). The polarized state of the debate on this issue is clearly demonstrated by the recent, strongly contrasting studies of Manning et al. (2006) and Fedo et al. (2006). Detailed geological maps of the southwestern extension of the island of Akilia are provided in Nutman et al. (2002b) and Manning et al. (2006). A brief sample description is given below.

Samples for this study were collected in 2004, with the purpose to confirm and further expand the earlier study of Dauphas et al. (2004a). Sample AK-04-01 is a greenish-black rock derived from the main ultramafic body in the southwestern extension of the island of Akilia, directly north of the quartz-pyroxene rock outcrop. It should represent the igneous endmember for Fe-isotope studies. Samples AK-04-03 and AK-04-04 represent the exact north-eastern contact of the quartz-pyroxene rock and amphibolites and ultramafic rocks. Samples AK-04-05 and AK-04-06 represent the exact southwestern contact of the quartz-pyroxene rock and amphibolites. This southwestern contact consists of a garnet-rich zone. Sample AK-04-07 represents the fine-grained part of the quartz-pyroxene rock. It was

Table 1
Mineral mode analyses (% of surface area) of selected metacarbonates and BIFs from the ISB

	Carbonates			Amphiboles			Chlorite	Muscovite	Biotite	Garnet	Magnetite	Plagioclase	Fe-oxihydroxide	Quartz	Hornblende	Graphite	Apatite	Allanite	Pyrite	Rutile	Chromite
	Calcite	Dolomite	Mg-siderite	Grun/Cumm	Trem/Act	Antoph															
IS-04-01			70	10							15		5				<1		<1		
IS-04-02			70	5			15				0		10							<1	
IS-04-03			60		20		5				0		15							<1	
IS-04-05	20	50			30						0										
IS-04-07				15						5	50					<2	<1				
IS-04-08				15			35			35	10		5			<2	<1				
IS-04-09				15			25				30					<2	<1				
IS-04-10			30	15			20				33		2			<2	<1				
IS-04-11			30	10			35				23		2			<2	<1				
IS-04-06	5			10							35			50							
9-1A1B				7			3				30			58					2		
9-1A2B				10							35			55							
10-1A2B	10			10							30			50							
10-1A3B	10			10							35			45							
AL-6-2		<1		<1	10	3			<1		25			60	<1				2		
AL-04-G18	30	40			30												<1		<1		
AL-04-G23	25	5						20	15					35			<1	<1			

collected several meters north (along the banding direction) of the actual locality of the well documented fine-grained quartz-pyroxene rock samples G91-26 (ANU92-197) and SM/GR/97/5 that were analyzed in Dauphas et al. (2004a). The general mineralogy of these samples is quartz, grunerite, hornblende, clinopyroxene, orthopyroxene, actinolite, magnetite, and minor pyrite, chalcopyrite, apatite and calcite. Sample AK-04-08 is derived from the coarse-grained bulk of middle part of the quartz-pyroxene rock, and is similar to the sample AK-98 studied in Dauphas et al. (2004a). Finally, sample ING-04-01 was collected from the Akilia Association on the island of Innersuartuut, about 10 km south of the island of Akilia. This represents a small, 2 m long quartz-pyroxene lens in the southern part of the island, and occurs in the close vicinity of the location for sample 171770 that was analyzed in Dauphas et al. (2004a).

3. METHODS

Major and trace element analyses of bulk samples (results of which are reported in Table 2 and Electronic annex) were performed at the Service d'Analyse des Roches et des Minéraux (SARM) of the Centre de Recherches Pétrographiques et Géochimiques (France). After fusion with lithium metaborate and dissolution in acid, major elements were analyzed on a Jobin-Yvon JY 70 ICP-AES. Trace element concentrations were measured by ICP-MS on a Perkin-Elmer ELAN 5000. Because of its low concentration, there are few Ti measurements available in the literature of chemical sediments or metasomatic rocks from Akilia, Innersuartuut, and the ISB (McGregor and Mason, 1977; Appel, 1980; Nutman et al., 1984, 1996; Dymek and Klein, 1988; Dauphas et al., 2004a; Fedo and Whitehouse, 2002a; Cates and Mojzsis, 2006). For this reason, this element was measured separately on a Beckman DU 62 spectrophotometer after digestion in HF–$HClO_4$ (detection limit 0.0006 wt% TiO_2). Detection limits and uncertainties are available at http://www.crpg.cnrs-nancy.fr/SARM/.

The procedures used in our laboratory for preparing samples, purifying Fe, and analyzing the Fe isotopic composition have been presented in detail in other contributions (Dauphas et al., 2004b, 2007; Dauphas and Rouxel, 2006) and will be briefly reviewed here. After cleaning with acetone, bulk samples were powdered in an agate mortar. Between each sample, the mortar was wiped with a moist disposable cloth, rinsed with milli-Q water, and high purity quartz was ground to avoid cross-contamination. We also sampled individual mineral phases using a microdrilling apparatus (MicroMill, New Wave Research) equipped with a carbide mill bit (Brasseler scriber H1621.11, see Dauphas et al., 2007 for details). After backscattered electron imaging of a polished section on a JEOL JSM-5800LV SEM, magnetite was drilled out of the Isua BIF IS-04-06 (Fig. 5). Mineral phases (magnetite, garnet, and Mg-siderite) were also drilled out of the Isua metacarbonate AL-44 (Fig. 6, Lepland et al., 2002; van Zuilen et al., 2003). Before microdrilling, the drilling locations were covered with a drop of milli-Q water. In addition to the minerals that were directly aimed for sampling, the slurries produced by microdrilling always contained minor amounts of other minerals (magnetite in garnet, magnetite in carbonate, and garnet-carbonate in magnetite). The drilled material in suspension in water was further purified using a teflon-coated magnetic stirring bar. The resulting fractions were almost monomineralic (>90%). Wet sieving was used on metacarbonates to separate a 210–420 μm size fraction, which was then subject to hand picking of magnetite and amphibole/chlorite to assess the effect of weathering on the isotopic composition of Fe in carbonates.

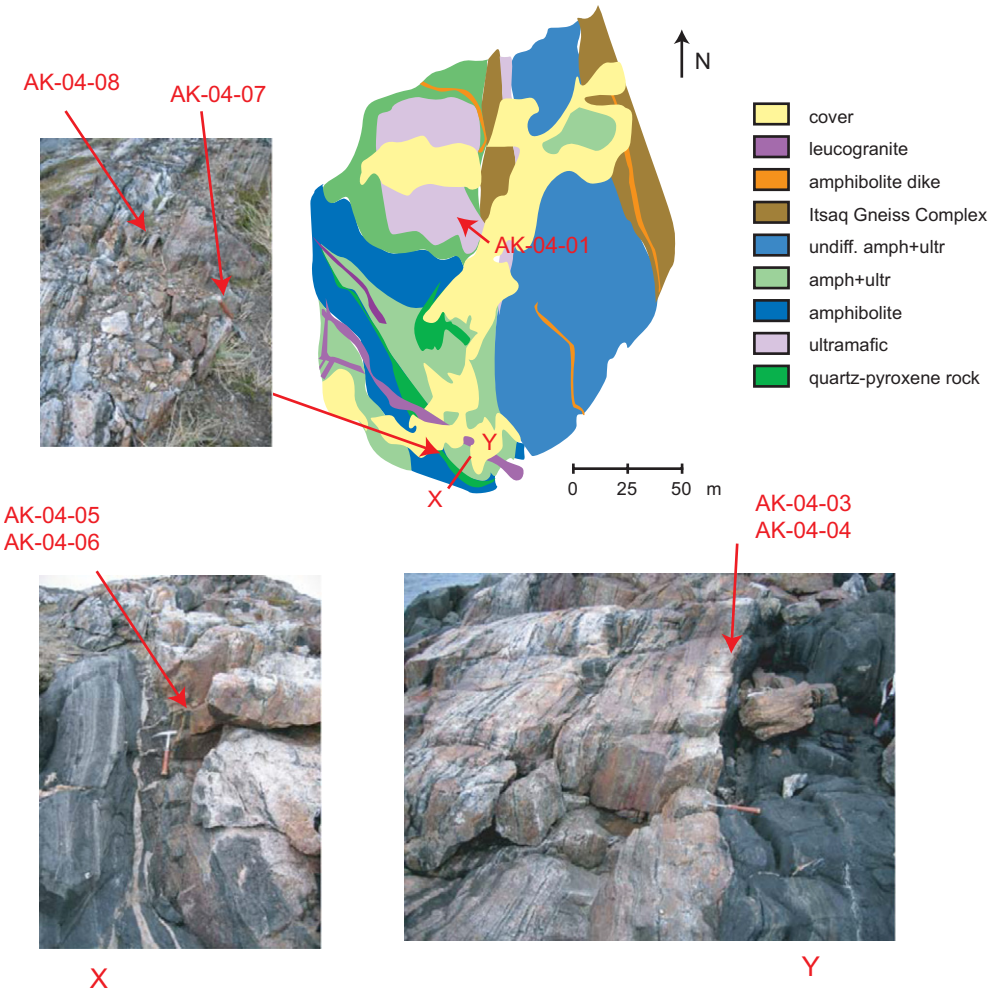

Fig. 4. Geologic map of the southwestern promontory of the island of Akilia, southern West Greenland (redrawn from Manning et al., 2006; also see Nutman et al., 2002b). This part of the island represents one of several small supracrustal enclaves within an early Archean orthogneiss complex. Near the southern tip of the promontory a five meter wide quartz-pyroxene rock occurs within an igneous surrounding (sample AK-04-01 from an ultramafic body to the north). A profile (X–Y) from the southwestern contact (samples AK-04-05 and AK-04-06) to the northeastern contact (samples AK-04-03 and AK-04-04) is shown in detail (view towards the north-west). Several meters to the northwest, along the banding direction two samples were collected; sample AK-04-07 (fine-grained part) and sample AK-04-08 (coarse-grained part).

Powdered bulk samples and mineral separates (typically <10 mg) were digested in Teflon beakers using the following sequence of acid addition–heating in closed beakers for a total of ~5 h at 100 °C + evaporation under a heat lamp: (i) 1 mL HF + 0.5 mL HNO_3 + few drops of $HClO_4$, (ii) 0.25 mL HNO_3 + 0.75 mL HCl + few drops of $HClO_4$, (iii) 0.5 mL HNO_3 + 1 mL HCl + few drops of $HClO_4$ (all acids are concentrated solutions). The samples were finally dissolved in 0.2–0.5 mL of 6 M HCl before loading on a column filled with 1 mL of AG1-X8 200–400 mesh anion exchange resin. Matrix elements and direct isobars of Fe were eluted with 8 mL of 6 M HCl and Fe was recovered using 9 mL of 0.4 M HCl. The eluate containing Fe was evaporated to dryness and loaded on a second column for further purification using the same elution sequence. The yield is close to 100% and the chemistry blank is negligible compared to the amount of Fe in the samples.

The Fe isotopic composition was measured in 0.45 M HNO_3 at a concentration of 2 ppm on an Isoprobe (Micromass) multi-collector inductively coupled plasma mass spectrometer (MC-ICPMS, Isotope Geochemistry Laboratory, Field Museum). The sample solutions were introduced in the mass spectrometer using a Cetac Aridus desolvating system. Instrumental mass fractionation was corrected by standard bracketing with the reference material IRMM-014 (Taylor et al., 1992). Variations in the Fe isotopic compositions of natural samples relative to the reference material are calculated using,

$$\delta^{56}\mathrm{Fe} = \left(\frac{^{56}\mathrm{Fe}/^{54}\mathrm{Fe}_{\mathrm{Sample}}}{^{56}\mathrm{Fe}/^{54}\mathrm{Fe}_{\mathrm{IRMM\text{-}014}}} - 1\right) \times 10^3.$$

To facilitate inter-laboratory and inter-element comparisons, we also calculate the isotopic fractionation in permil per atomic mass unit deviation relative to the composition of IRMM-014 (‰/amu),

$$F_{\mathrm{Fe}} = \delta^{56}\mathrm{Fe}/(56\text{–}54).$$

Error bars are 95% confidence intervals estimated based on repeated analyses of the reference material by standard bracketing as is done for the samples. Most sample analyses were replicated at least once (and sometimes more) from acid digestion to isotopic analysis (Table 3) and the results agree with each other.

Table 2
Major and selected trace element concentrations of igneous rocks, metacarbonates, and BIFs from Isua, Akilia, and Innersuartuut (southern West Greenland)

	AK0401	AK0403	AK0406	AK0404	AK0405	AK0407	AK0408	lng04-01	IS0401	IS0402	IS0403	IS0405	IS0407	IS0408	IS0409	IS0410	IS0411	AL04G18	AL04G23
Ce (ppm)	6.009	22.74	11.75	19.97	2.261	0.551	0.431	7.674	0.584	1.511	12.08	2.079	4.693	8.005	15.82	16.58	15.61	2.817	31.27
Dy (ppm)	2.272	4.076	5.261	9.918	0.232	0.169	0.095	1.288	0.206	0.216	4.382	0.364	3.151	11.6	2.5	1.1	2.6	0.524	0.953
Er (ppm)	1.212	2.292	2.847	4.818	0.147	0.098	0.054	0.574	0.195	0.14	2.641	0.26	2.044	6.174	1.43	0.776	1.704	0.373	0.465
Eu (ppm)	0.612	0.675	0.906	0.782	0.219	0.056	0.049	0.135	0.065	0.138	1.159	0.341	0.636	0.713	0.503	0.743	1.549	0.365	0.558
Ga (ppm)	8.573	20	27.86	17.22	16.17	2.555	0.308	2.581	0.869	0.628	0.864	0.536	7.441	30.61	9.212	5.239	5.753	0.326	12.85
Gd (ppm)	2.301	4.417	4.853	11.11	0.134	0.134	0.077	1.547	0.189	0.237	3.94	0.403	2.305	7.295	2.83	1.19	2.313	0.551	1.459
Ho (ppm)	0.443	0.81	1.023	1.829	0.05	0.032	0.019	0.219	0.051	0.047	0.935	0.091	0.683	2.328	0.518	0.242	0.576	0.125	0.167
La (ppm)	2.202	6.661	3.39	2.9	1.571	0.197	0.218	2.238	0.283	1.074	5.738	2.103	2.206	3.368	8.218	9.548	8.912	2.937	15.12
Lu (ppm)	0.17	0.345	0.525	0.579	0.024	0.017	0.008	0.061	0.059	0.035	0.402	0.03	0.31	0.772	0.199	0.178	0.252	0.041	0.065
Nd (ppm)	5.332	17.91	9.309	31.78	0.776	0.292	0.226	5.752	0.408	0.657	7.614	0.872	2.698	5.011	8.863	6.697	6.954	1.2	13.58
Pr (ppm)	0.973	3.709	1.894	5.103	0.245	0.074	0.052	1.236	0.082	0.162	1.633	0.206	0.611	1.083	1.977	1.798	1.774	0.287	3.649
Sm (ppm)	1.791	4.765	3.45	11.26	0.127	0.089	0.054	1.685	0.132	0.174	2.427	0.187	0.828	2.106	2.208	1.219	1.688	0.299	2.19
Tb (ppm)	0.369	0.684	0.863	1.71	0.029	0.022	0.014	0.233	0.029	0.034	0.658	0.057	0.459	1.632	0.416	0.173	0.395	0.077	0.187
Tm (ppm)	0.173	0.354	0.447	0.654	0.022	0.014	0.007	0.075	0.036	0.024	0.381	0.033	0.298	0.872	0.202	0.125	0.253	0.047	0.066
Y (ppm)	11.82	22.85	30.18	51.17	1.685	1.262	0.756	7.536	2.648	1.938	36.39	7.031	26.33	74.58	19.52	8.794	19.94	8.975	5.137
Yb (ppm)	1.15	2.343	3.146	4.078	0.154	0.101	0.048	0.452	0.331	0.191	2.555	0.193	1.95	5.379	1.291	0.985	1.643	0.266	0.422
SiO_2 (%)	48.22	43.15	50.24	47.00	70.64	68.89	94.37	0.06	0.06	1.97	4.27	17.80	4.58	26.04	12.51	4.85	0.13	21.77	62.58
Al_2O_3 (%)	6.24	14.29	14.94	7.35	17.96	0.12	0.04	0.72	0.04	0.40	0.62	0.19	1.37	16.30	6.05	1.78	2.36	<D.L.	9.28
Fe_2O_3 (%)	10.83	16.60	14.84	18.30	0.19	22.02	1.97	10.83	33.77	33.97	35.32	3.69	85.15	44.58	67.73	71.03	65.41	4.60	3.52
MnO (%)	0.20	0.28	0.46	0.28	0.01	0.29	0.06	0.27	0.90	0.30	0.27	0.60	2.24	1.65	2.17	2.49	3.16	0.51	0.26
MgO (%)	18.07	8.50	6.78	10.34	0.00	4.85	0.0050	0.00	23.60	23.66	21.43	16.69	0.015	50.00	5.67	6.68	0.00	16.62	3.93
CaO (%)	13.02	11.90	8.35	11.62	5.71	2.58	1.53	3.53	0.28	0.49	0.48	27.24	0.15	1.39	0.99	0.70	0.41	27.81	8.04
Na_2O (%)	0.79	1.81	2.80	0.99	4.51	<D.L.	<D.L.	<D.L.	<D.L.	<D.L.	<D.L.	<D.L.	<D.L.	<D.L.	<D.L.	<D.L.	<D.L.	<D.L.	<D.L.
K_2O (%)	0.17	0.50	0.38	0.23	0.17	<D.L.	<D.L.	<D.L.	<D.L.	<D.L.	<D.L.	<D.L.	<D.L.	<D.L.	<D.L.	<D.L.	<D.L.	<D.L.	3.66
TiO_2[b] (%)	0.50	1.05	0.54	1.36	0.0029	0.0028	0.0009	0.023	0.0031	0.0055	0.58	0.010	0.038	1.83	0.16	0.053	0.067	0.0009	0.24
P_2O_5 (%)	0.06	0.04	0.04	0.06	<D.L.	0.06	<D.L.	0.03	0.04	0.04	0.04	0.02	0.09	0.04	0.74	0.22	0.10	0.02	0.10
LOI (%)	1.74	0.97	1.05	1.35	0.43	1.20	0.76	0.84	40.94	40.04	36.81	32.36	4.12	2.86	4.35	10.85	12.81	28.94	8.19
Total (%)	99.83	99.08	100.42	98.87	99.65	100.00	99.58	100.06	99.89	100.86	99.82	98.60	98.54	100.19	100.36	98.67	99.45	100.26	99.79

	IS0406	9-1A1B	9-1A2B	10-1A2B	10-1A3B	AL6-1b	AL6-2b	AL04-G22	ANU92-197 [1]	SM/GR/97/2[a]	SM/GR/97/3[a]	SM/GR/97/4[a]	SM/GR/97/5[a]	SM/GR/97/6[a]	SM/GR/97/7[a]	SM/GR/97/9[a]	ING-171770[a]	ING-171771[a]	AK-98[a]
Ce (ppm)	3.302	0.798	0.607	2.249	1.481	4.084	1	0.488	1.451	17.72	5.179	9.144	2.356	2.445	37.73	12.68	16.83	6.272	0.815
Dy (ppm)	0.607	0.142	0.368	0.38	0.483	1.386	0.448	0.263	0.229	1.645	2.326	1.624	0.433	1.284	2.543	0.975	3.856	1.367	0.428
Er (ppm)	0.47	0.118	0.301	0.28	0.361	1.15	0.36	0.15	0.142	0.871	1.229	1.081	0.262	0.842	1.343	0.421	1.797	0.895	0.323
Eu (ppm)	0.248	0.045	0.074	0.182	0.181	0.228	0.169	0.033	0.11	0.59	0.551	0.353	0.136	0.24	0.921	0.195	0.276	0.66	0.062
Ga (ppm)	0.875	0.997	1.738	1.255	1.032	14.36	1.446	1.142	0.782	22.43	9.203	16.11	0.705	9.923	20.67	2.196	4.627	6.774	0.76
Gd (ppm)	0.523	0.136	0.213	0.279	0.337	0.699	0.299	0.194	0.231	1.938	2.322	1.31	0.381	0.993	2.943	1.415	4.27	1.394	0.293
Ho (ppm)	0.152	0.035	0.093	0.09	0.122	0.343	0.111	0.055	0.051	0.313	0.459	0.348	0.091	0.284	0.48	0.167	0.692	0.305	0.101
La (ppm)	2.507	0.541	0.341	1.313	0.91	1.4	0.764	0.198	0.564	7.083	1.584	3.818	0.646	1.058	17.66	3.891	4.709	1.88	0.252
Lu (ppm)	0.083	0.019	0.038	0.047	0.057	0.199	0.061	0.022	0.021	0.133	0.17	0.188	0.04	0.149	0.2	0.051	0.238	0.149	0.064
Nd (ppm)	1.443	0.395	0.333	0.891	0.682	1.868	0.434	0.317	0.681	9.883	5.4	4.808	1.607	1.838	16.92	8.478	13.3	4.973	0.678
Pr (ppm)	0.36	0.095	0.073	0.232	0.165	0.492	0.097	0.068	0.172	2.355	0.936	1.191	0.363	0.358	4.347	1.954	2.787	1.029	0.133
Sm (ppm)	0.309	0.08	0.105	0.176	0.188	0.483	0.137	0.102	0.168	2.246	1.906	1.151	0.396	0.686	3.449	1.895	4.105	1.265	0.219
Tb (ppm)	0.079	0.02	0.045	0.05	0.065	0.169	0.061	0.04	0.036	0.281	0.379	0.237	0.066	0.186	0.434	0.194	0.687	0.216	0.059
Tm (ppm)	0.069	0.018	0.045	0.043	0.055	0.178	0.055	0.02	0.02	0.128	0.175	0.171	0.04	0.136	0.188	0.055	0.246	0.134	0.052
Y (ppm)	7.686	1.626	3.377	3.485	5.172	10.22	4.76	1.756	1.76	9.3	12.34	10.36	2.946	7.833	13.97	5.406	21.26	10.29	3.495

Yb (ppm)	0.492	0.115	0.303	0.283	0.362	1.212	0.364	0.142	0.134	0.829	1.109	1.178	0.256	0.947	1.28	0.338	1.599	0.878	0.371
SiO_2 (%)	62.53	88.77	81.56	46.41	55.92	57.43	50.61	90.08	78.11	63.38	46.32	51.12	81.11	45.95	56.89	77.51	71.21	42.13	86.41
Al_2O_3 (%)	0.50	0.35	0.12	29.68	0.05	12.37	0.06	0.46	<D.L.	16.81	5.47	17.2	<D.L.	9.63	16.14	0.5	1.52	1.88	<D.L.
Fe_2O_3 (%)	31.15	9.32	16.20	3.33	38.07	12.54	46.53	5.25	13.92	5.18	14.41	9.09	9.41	11.05	8.34	10.8	16.9	50.52	9.44
MnO (%)	0.14	0.06	0.06	0.05	0.11	0.08	0.08	0.07	0.19	0.07	0.19	0.13	0.2	0.17	0.14	0.29	0.5	0.23	0.25
MgO (%)	2.08	0.53	1.37	1.83	4.22	7.63	2.22	0.91	3.32	2.84	20.64	8.79	3.47	24.11	4.8	3.6	4.7	3.79	2.69
CaO (%)	2.87	0.09	0.93	16.04	1.04	0.26	0.79	0.11	5.31	5.03	10.27	6.63	5.53	5.13	7.37	7.47	6.39	3.09	1.1
Na_2O (%)	<D.L.	<D.L.	<D.L.	1.66	<D.L.	1.21	<D.L.	<D.L.	<D.L.	4.13	0.2	3.79	<D.L.	0.2	3.94	<D.L.	<D.L.	<D.L.	<D.L.
K_2O (%)	0.06	<D.L.	<D.L.	0.13	<D.L.	3.08	<D.L.	<D.L.	<D.L.	1.55	<D.L.	1.81	<D.L.	<D.L.	0.67	<D.L.	<D.L.	<D.L.	<D.L.
TiO_2 [b] (%)	0.0050	0.0080	0.015	0.0070	0.0024	0.54	0.0078	0.038	0.002	0.48	0.62	0.33	0.002	0.31	0.73	0.015	0.046	0.14	0.002
P_2O_5 (%)	0.05	0.02	0.04	<D.L.	0.05	0.15	0.04	<D.L.	<D.L.	0.08	<D.L.	<D.L.	<D.L.	0.04	0.12	<D.L.	<D.L.	<D.L.	<D.L.
LOI (%)	0.87	0.46	0.16	0.42	1.08	4.15	0.34	1.61	−0.48	0.58	1.63	1.18	0.23	3.55	0.78	−0.41	−0.79	−1.69	−0.06
Total (%)	100.26	99.61	100.45	99.54	100.54	99.43	100.68	98.53	100.37	100.1	99.71999	100.05	99.95	100.14	99.9	99.76	100.46	100.07	99.83001

The complete data set is available as Electronic annex.
<D.L. means that the concentration is below detection limit. LOI stands for loss on ignition. Visit http://www.crpg.cnrs-nancy.fr/SARM/ for detection limits and precisions.
[a] Iron isotope analyses and sample descriptions are available in Dauphas et al. (2004a).
[b] Measured separately by spectrophotometry.

The carbonates that we analyzed contain less Fe or have different chemical compositions compared to samples that we usually process in our laboratory. For this reason great care was taken to validate our results. The samples that were selected to test the method are (i) AC-E, a granite geostandard from Ailsa Craig island (SW Scotland) which only contains 1.8 wt% of Fe (Govindaraju, 1994), (ii) IS-04-05, a Fe-poor carbonate from the western part of the ISB that has the most negative Fe isotopic composition of all carbonates measured in this study (Tables 3 and 4), and (iii) IS-04-07, a Fe-rich carbonate from the Eastern part of the ISB that has the most positive Fe isotopic composition of all carbonates measured in this study (Tables 3 and 4). After dissolution of the test samples, we passed them through a first column, recovered matrix elements (6 M HCl fraction) and the Fe eluate (0.4 M HCl fraction). The matrix fraction was passed through a second column to get rid of residual Fe, if any. The Fe-free matrix was doped with 100 μg of IRMM-014. This solution of Fe-free matrix + IRMM-014 was processed using our usual protocol for purifying Fe. Iron that was eluted from the first column was passed through a second column and the Fe eluate was split into two fractions. Half was kept for direct isotopic measurement and the other half was passed through a third column. So from one sample aliquot we generated three solutions: (i) IRMM-014 that had been mixed with the Fe-free sample matrix and processed through two columns, (ii) sample Fe processed through two columns, and (iii) sample Fe processed through three columns. The potential sources of artifacts in Fe isotopic analyses are isotopic fractionation during column chromatography, changes in the instrumental mass bias due to the presence of matrix elements, and isobaric interferences such as $^{54}Cr^+$ or $^{58}Ni^+$. All samples plot on a single fractionation line ($\delta^{57}Fe \approx 1.5 \times \delta^{56}Fe$, the slope and intercept of the linear regression of the data points in Table 3 are 1.530 ± 0.046 and 0.008 ± 0.026, respectively) so the presence of uncorrected isobaric interferences can be excluded. The solutions of matrix + IRMM-014 have isotopic compositions of 0‰/amu within uncertainties (-0.022 ± 0.070 and 0.010 ± 0.029‰/amu for IS-04-05 and IS-04-07, respectively), so matrix effect and chromatographic fractionation can be ruled out as well. Finally, the samples processed through three columns have the same compositions as those passed through two columns (0.151 ± 0.054 vs 0.134 ± 0.054, -0.377 ± 0.081 vs -0.350 ± 0.081, and 0.392 ± 0.029 vs 0.377 ± 0.029 ‰/amu for AC-E, IS-04-05, and IS-04-07, respectively) confirming that the yield is close to 100% and that the purification procedure does not fractionate Fe isotopes outside of analytical uncertainties. Replicate analyses of the three test samples give identical results despite different amounts of Fe loaded on the column. From these tests, we can safely conclude that the isotopic variations that we document in metacarbonates are real and are not artifacts introduced in the laboratory.

4. RESULTS

4.1. REE + Y

Loss on ignition (LOI) and a total of 53 elements were measured in 38 samples (Table 2 and Electronic annex). In almost all cases, element abundances sum up to 100% (within 1%).

Study of REE + Y chemistry in the modern ocean (Elderfield, 1988; Byrne and Kim, 1990; Byrne and Lee, 1993; Zhang et al., 1994; Bau, 1996, 1999; Nozaki et al., 1997; Quinn et al., 2004) provides important clues for understanding the formation of BIFs (Dymek and Klein, 1988; Jacobsen and Pimentel-Klose, 1988; Derry

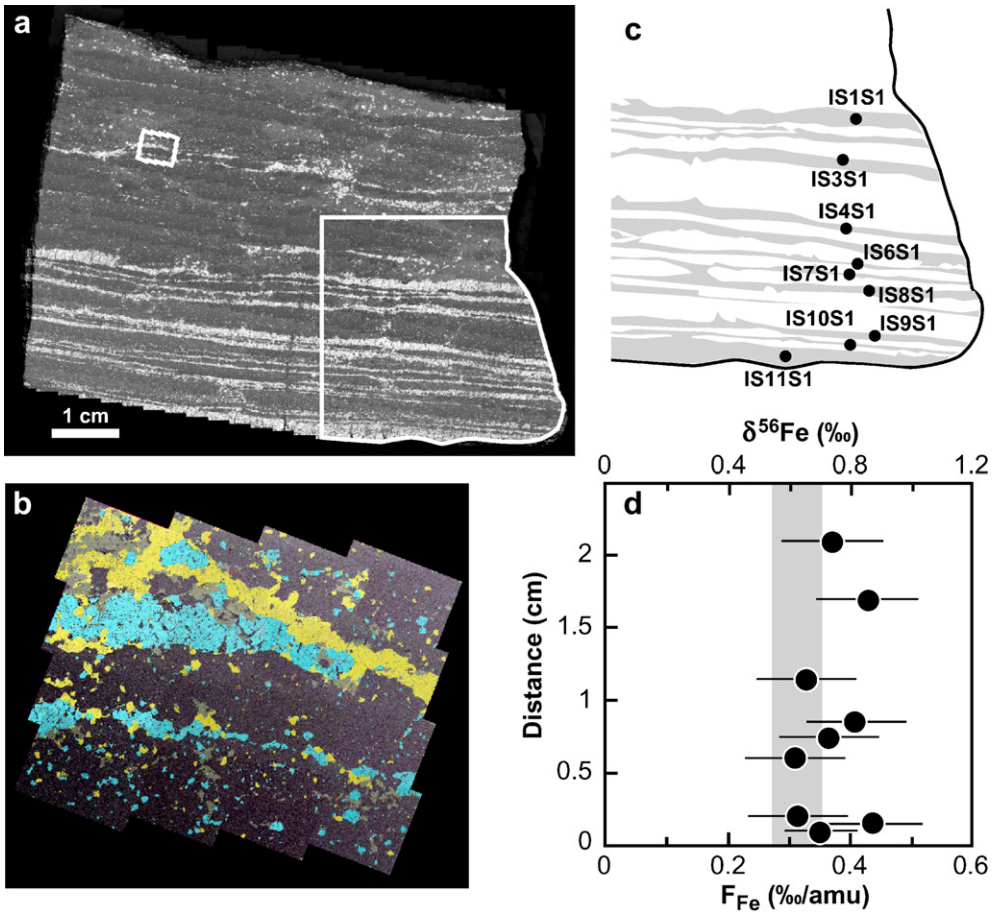

Fig. 5. Petrographic context and Fe isotopic composition (relative to IRMM-014) of micro-drilled magnetite from the Isua BIF IS-04-06 (Table 5). (a) Mosaic backscattered electron image of IS-04-06. The scale bar is 1 cm. The white bands are composed of magnetite while the rest comprises silicates and carbonates. The areas contoured in white are shown in (b) and (c). (b) False color CMYK mosaic obtained by superposing chemical X-ray maps of iron (cyan, C), phosphorus (magenta, M), calcium (yellow, Y), and silicon (black, K). The blue bands are composed of magnetite, the red spots are apatite, the yellow band is calcite, the light grey areas are amphibole, and the dark grey areas are quartz (see Section 2.1 for details on the mineralogy). (c) Localisation map of magnetite bands sampled by micro-drilling for Fe isotope analyses (see a for scale of sampling). (d) Fe isotope results relative to IRMM-014 (Table 5). The distance is taken from the bottom of (a). The grey band shows the weighted average of bulk measurements of IS-04-06. The MSWD is 1.39, within the two-sided 95% interval predicted from the reduced χ^2 distribution for $n-1=8$ degrees of freedom (0.27–2.19). (For interpretation of the references to color in this figure legend, the reader is referred to the web version of this paper.)

and Jacobsen, 1990; Shimizu et al., 1990; Danielson et al., 1992; Alibert and McCulloch, 1993; Bau and Möller, 1993; Bau and Dulski, 1996; Bolhar et al., 2004; Frei and Polat, 2007). The REE + Y pattern of seawater depends on several factors. The source of REE + Y in modern oceans is continental run-off and eolian transport (post-Archean Australian Shale is a good proxy). In the Archean, the source is not clearly defined but there is no question that it included a high-temperature hydrothermal component that imparted a positive Eu anomaly to Eoarchean BIFs relative to chondrites (Dymek and Klein, 1988; Derry and Jacobsen, 1990; Danielson et al., 1992; Bau and Möller, 1993). The main vector for removal of REE + Y from the oceans is scavenging by particulate matter. This is controlled by competition between solution (e.g., CO_3^{2-}) and surface (e.g., solid oxyhydroxide) complexation of trivalent REE (Elderfield, 1988; Byrne and Kim, 1990; Quinn et al., 2004). Byrne and Kim (1990) interpret the enrichment in HREE relative to LREE in modern seawater to reflect a stronger increase with atomic number of solution complexation relative to surface complexation. HREEs are less easily scavenged, have a longer residence time, and therefore higher concentrations in seawater than LREEs. La and Y depart from this smooth trend of solution/surface complexation with atomic mass number (Byrne and Kim, 1990; Bau, 1999; Quinn et al., 2004) and as a result show up as positive anomalies relative to neighbor REEs in modern seawater (Byrne and Lee, 1993; Zhang et al., 1994; Bau, 1996; Nozaki et al., 1997). Bolhar et al. (2004) and Frei and Polat (2007) identified several features that can be used to distinguish a marine deposit from a metasomatic rock. These features include: (i) concave upward REE pattern, (ii) positive $La/La* = La_N/(Ce_N^2/Pr_N)$ anomaly, (iii) positive $Eu/Eu^* = Eu_N/(Sm_N \times Gd_N)^{0.5}$ anomaly, and (iv) suprachondritic Y/Ho ratio.

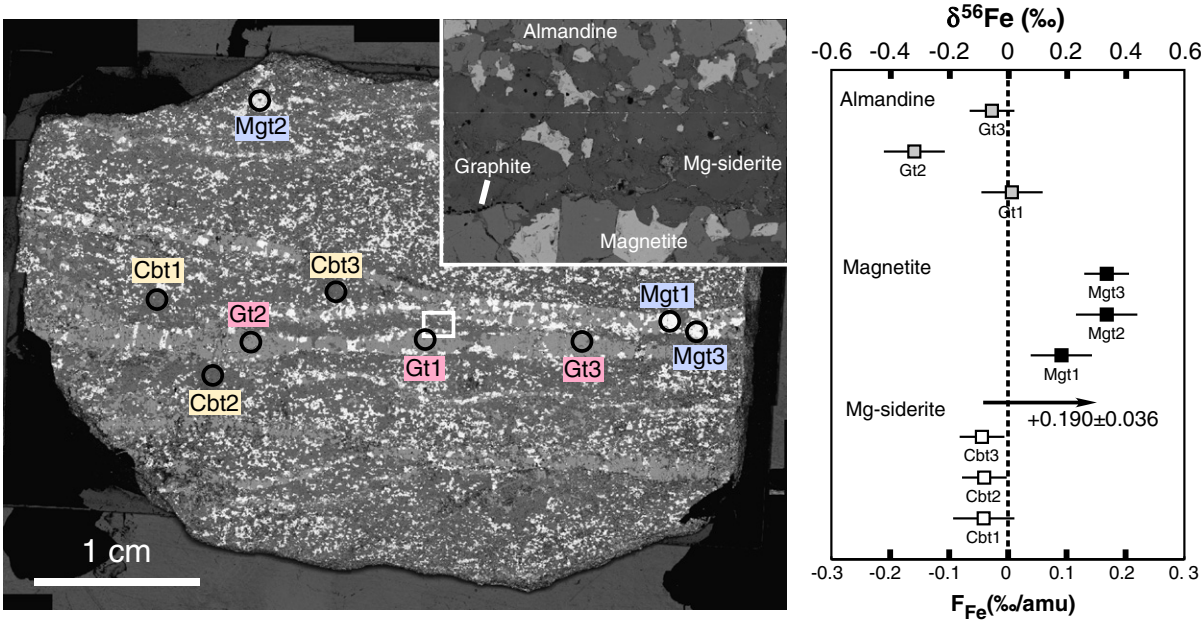

Fig. 6. Petrographic context and Fe isotopic composition (relative to IRMM-014) of individual phases in the Isua metacarbonate AL-44. The left panel shows a backscattered electron mosaic of the studied section with locations of areas sampled with the microdrill (see text for more details). The inset is a back scattered electron image of the area indicated by the white square showing textural relationships between almandine, Mg-siderite, magnetite, and graphite. The Fe isotopic composition relative to IRMM-014 is shown in the right panel. Almandine has similar Fe isotopic composition compared to Mg-siderite and both phases have light compositions relative to magnetite (~0.2‰/amu). This probably reflects inter-mineral isotope fractionation at ~550 °C (Fig. 14).

Yttrium and Holmium are twin elements that have very similar chemical behaviors during melting and crystallization (Pack et al., 2007) but can be fractionated in aqueous fluids (Bau, 1996). Mafic igneous rocks have close to chondritic Y/Ho ratios (26.22 ± 0.40; Jochum et al., 1986, 1989; Pack et al., 2007; following the usual practice, we report this ratio in g/g, see Fig. 7 for conversion to mol/mol) while modern seawater has high and variable Y/Ho ratio, ranging from ~40 to 70 (Byrne and Lee, 1993; Zhang et al., 1994; Bau, 1996; Nozaki et al., 1997). Igneous rocks from Isua, Akilia, and Innersuartuut have close to chondritic Y/Ho ratio (average 27.44 ± 0.91, $n = 73$, Table 2, Fig. 7, and also data in McGregor and Mason, 1977; Nutman et al., 1996; Fedo and Whitehouse, 2002a; Polat et al., 2002; Komiya et al., 2004; Cates and Mojzsis, 2006). In Qtz-Px rocks from Akilia and Innersuartuut, the Y/Ho ratio is correlated with the logarithm of the Fe/Ti ratio (Fig. 7, the slope of the correlation Y/Ho (g/g) $= a \,\mathrm{Log}\, \mathrm{Fe/Ti}$ (mol/mol) $+ b$ is significantly different from zero, $a = 2.52 \pm 1.07$, $n = 29$). A similar correlation may also exist for metacarbonates from Isua but this is not statistically resolvable. This broad correlation is consistent with mixing between igneous and chemical sedimentary end-members (Fig. 7 shows the mixing trajectory between SM/GR/97/4 and AK-04-07, gabbroic and fine-grained Qtz-Px rocks from Akilia, respectively).

In the following discussion on trace element signatures, we limit ourselves to samples with Fe/Ti > 1000 because those are most likely to preserve original signatures of putative chemical sediments, least affected by igneous admixtures (through tectonic reworking or deposition of detrital sediments and volcanic ashes). Indeed, *bona fide* BIFs have much higher Fe/Ti ratios than igneous rocks (e.g., 10,346 for IF-G, a well-characterized BIF geostandard from Isua, Govindaraju, 1994 vs <60 for most igneous rocks from SW Greenland, Fig. 7). The Fe/Ti ratio is also useful because it is a potential proxy for Fe mobilization and transport. For instance, altered oceanic basalts are enriched in the heavy isotopes of Fe but this is associated with a reduction in the Fe/Ti ratio (Rouxel et al., 2003), which is opposite to what was observed by Dauphas et al. (2004a) in Qtz-Px rocks from the island of Akilia. We adopted a threshold of 1000 based on the mixing trajectory between SM/GR/97/4 and AK-04-07 (Fig. 7). Even if the Fe/Ti ratio of AK-04-07 were reduced from 8008 to 1000 mol/mol due to the addition of SM/GR/97/4, the Y/Ho ratio would only be modified from 39.3 to 35.5 (Fe/Ti = 29 mol/mol and Y/Ho = 29.8 g/g for the end member SM/GR/97/4).

Adopting a Fe/Ti threshold of >1000 mol/mol, the average Y/Ho ratios of Qtz-Px rocks from Akilia/Innersuartuut and BIFs and Fe-rich metacarbonates from Isua are 35.6 ± 2.3, 43.9 ± 5.9, and 42.0 ± 15.2 g/g, respectively. All these values are higher than chondritic and surrounding igneous rocks (~26–27) and fall close to the range of values documented for modern seawater (40–70).

We normalize all REE concentrations to CI1 chondrites (Anders and Grevesse, 1989; see Bau and Dulski, 1996, for pros and cons of the chondrite and shale normalizations).

For mafic and ultramafic rocks from the island of Akilia, we consider only high quality measurements where the whole suite of REEs was measured (Fig. 8; data in Table 2, Fedo and Whitehouse, 2002a). These rocks have on average chondritic composition but HREEs show less scatter in

Table 3
Iron isotopic compositions of bulk igneous rocks, metacarbonates, and BIFs from Isua, Akilia, and Innersuartuut (southern West Greenland)

Type	Sample	Description	Fe (mol g^{-1})	δ^{56}Fe (‰)	δ^{57}Fe (‰)	F_{Fe} (‰/amu)
Igneous	AK-04-01	Akilia, Ultramafic N of Qtz-Px unit	0.00135	−0.037 ± 0.126	−0.033 ± 0.287	−0.019 ± 0.063
BIF/igneous?	AK-04-03 dark	Akilia N contact Qtz-Px unit		0.307 ± 0.104	0.533 ± 0.370	0.154 ± 0.052
				0.295 ± 0.155	0.611 ± 0.133	0.148 ± 0.078
	Average	AK-04-03 dark	0.00208	0.303 ± 0.086	0.602 ± 0.125	0.152 ± 0.043
BIF/igneous?	AK-04-06 dark	Akilia S contact Qtz-Px unit		0.081 ± 0.155	0.197 ± 0.134	0.041 ± 0.078
				−0.007 ± 0.048	−0.058 ± 0.121	−0.004 ± 0.024
	Average	AK-04-06 dark	0.00186	0.001 ± 0.046	0.057 ± 0.090	0.000 ± 0.023
BIF?	AK-04-04	Akilia Qtz-Px rock, N contact		0.337 ± 0.051	0.474 ± 0.147	0.169 ± 0.026
				0.315 ± 0.100	0.509 ± 0.131	0.158 ± 0.050
	Average	AK-04-04	0.00229	0.332 ± 0.045	0.494 ± 0.098	0.166 ± 0.023
BIF?	AK-04-05	Akilia Qtz/Px S contact Gt zone		0.259 ± 0.163	0.292 ± 0.315	0.130 ± 0.082
				0.214 ± 0.058	0.340 ± 0.138	0.107 ± 0.029
	Average	AK-04-05	0.0000238	0.219 ± 0.054	0.332 ± 0.127	0.110 ± 0.027
BIF?	AK-04-07	Akilia fine-grained Qtz-Px rock		0.856 ± 0.061	1.401 ± 0.273	0.428 ± 0.031
				0.903 ± 0.092	1.354 ± 0.177	0.452 ± 0.046
	Average	AK-04-07	0.00275	0.870 ± 0.051	1.368 ± 0.149	0.435 ± 0.025
BIF?	AK-04-08	Akilia coarse-grained Qtz-Px rock		0.382 ± 0.074	0.616 ± 0.248	0.191 ± 0.037
				0.376 ± 0.079	0.616 ± 0.166	0.188 ± 0.040
	Average	AK-04-08	0.000246	0.379 ± 0.054	0.616 ± 0.138	0.190 ± 0.027
BIF?	lng-04-01	Innersuartuut, Qtz-Px enclave		0.414 ± 0.066	0.737 ± 0.216	0.207 ± 0.033
				0.418 ± 0.082	0.638 ± 0.158	0.209 ± 0.041
	Average	lng-04-01	0.00135	0.416 ± 0.051	0.673 ± 0.128	0.208 ± 0.026
Metacarbonate	IS-04-01	Siderite SW of the belt		0.251 ± 0.063	0.321 ± 0.105	0.125 ± 0.032
				0.146 ± 0.157	0.208 ± 0.200	0.073 ± 0.079
	Average	IS-04-01	0.00422	0.236 ± 0.059	0.296 ± 0.093	0.118 ± 0.029
Metacarbonate	IS-04-02	Siderite NW of the belt		0.356 ± 0.157	0.550 ± 0.200	0.178 ± 0.079
				0.251 ± 0.207	0.374 ± 0.318	0.126 ± 0.104
	Average	IS-04-02	0.00425	0.318 ± 0.125	0.500 ± 0.169	0.159 ± 0.063
Metacarbonate	IS-04-03	Siderite NW of the belt		0.462 ± 0.212	0.778 ± 0.364	0.231 ± 0.106
				0.446 ± 0.079	0.760 ± 0.166	0.223 ± 0.040
	Average	IS-04-03	0.00442	0.448 ± 0.074	0.763 ± 0.151	0.224 ± 0.037
Metacarbonate	IS-04-05	Average from Table 1, W of the belt	0.00046	−0.742 ± 0.046	−1.096 ± 0.093	−0.371 ± 0.023
	IS-04-07	Average from Table 1, E of the belt	0.01064	0.759 ± 0.038	1.129 ± 0.074	0.380 ± 0.019
	IS-04-08	Siderite E of the belt		0.410 ± 0.092	0.633 ± 0.177	0.205 ± 0.046
				0.399 ± 0.037	0.583 ± 0.050	0.199 ± 0.018
	Average	IS-04-08	0.00557	0.400 ± 0.034	0.587 ± 0.048	0.200 ± 0.017
Metacarbonate	IS-04-09	Graphite-rich metacarbonate		0.327 ± 0.152	0.571 ± 0.291	0.164 ± 0.076
				0.285 ± 0.077	0.460 ± 0.201	0.143 ± 0.039
	Average	IS-04-09	0.00847	0.294 ± 0.069	0.496 ± 0.165	0.147 ± 0.034
Metacarbonate	IS-04-10	Siderite E of the belt (similar to IS-04-11)		0.276 ± 0.100	0.409 ± 0.131	0.138 ± 0.050
				0.295 ± 0.157	0.380 ± 0.200	0.148 ± 0.079
	Average	IS-04-10	0.00888	0.281 ± 0.084	0.400 ± 0.110	0.141 ± 0.042
Metacarbonate	IS-04-11	Graphite-rich metacarbonate		0.143 ± 0.076	0.217 ± 0.374	0.072 ± 0.038
				0.352 ± 0.152	0.593 ± 0.291	0.176 ± 0.076
				0.244 ± 0.100	0.361 ± 0.131	0.122 ± 0.050
			0.00818	0.204 ± 0.056	0.383 ± 0.114	0.102 ± 0.028
Metacarbonate	AL-04-G18	Heavily carbonated Amitsoq gneiss	0.000575	−0.901 ± 0.177	−1.456 ± 0.219	−0.451 ± 0.089
	Average	IS-04-11				
Metacarbonate	AL-04-G23	Carbonated Amitsoq gneiss	0.000440	−0.725 ± 0.177	−1.051 ± 0.219	−0.363 ± 0.089
BIF	IF-G	BIF geostandard	0.0069948	0.715 ± 0.11	1.125 ± 0.282	0.358 ± 0.055
BIF	IS-04-06	Fine-grained BIF, E of the belt		0.642 ± 0.100	0.974 ± 0.157	0.321 ± 0.050
				0.589 ± 0.157	0.921 ± 0.200	0.295 ± 0.079
			0.00389	0.627 ± 0.084	0.954 ± 0.123	0.313 ± 0.042
BIF	9-1A1	Banding of Qtz/Mgt		0.598 ± 0.066	0.848 ± 0.179	0.299 ± 0.033
	Average	IS-04-06				
	9-1A1B	Banding of Qtz/Mgt		0.423 ± 0.181	0.620 ± 0.341	0.212 ± 0.091
	Average	9-1A1	0.00117	0.577 ± 0.062	0.799 ± 0.158	0.289 ± 0.031
BIF	9-1A2	Banding of Qtz/Mgt		0.577 ± 0.098	0.918 ± 0.151	0.289 ± 0.049
	9-1A2B	Banding of Qtz/Mgt		0.434 ± 0.181	0.630 ± 0.341	0.217 ± 0.091
	Average	9-1A2	0.00203	0.545 ± 0.086	0.871 ± 0.138	0.272 ± 0.043
BIF	10-1A2	Pyrite BIF		1.093 ± 0.099	1.721 ± 0.152	0.547 ± 0.050
	10-1A2B	Pyrite BIF		0.903 ± 0.142	1.354 ± 0.228	0.452 ± 0.071
	Average	10-1A2	0.000416	1.031 ± 0.081	1.608 ± 0.126	0.515 ± 0.041

Table 3 (*continued*)

Type	Sample	Description	Fe (mol g^{-1})	δ^{56}Fe (‰)	δ^{57}Fe (‰)	F_{Fe} (‰/amu)
BIF	10-1A3	Pyrite BIF		0.773 ± 0.067	1.063 ± 0.179	0.387 ± 0.034
	10-1A3B	Pyrite BIF		0.734 ± 0.181	1.121 ± 0.341	0.367 ± 0.091
	Average	10-1A3	0.00476	0.768 ± 0.063	1.076 ± 0.158	0.384 ± 0.031
Schist	AL-6-1b	Pyrite containing banded qtz-chl schist	0.00157	0.010 ± 0.177	−0.046 ± 0.219	0.005 ± 0.089
BIF	AL-6-2b	Pyrite containing BIF 10 m from AL6-1	0.00582	1.030 ± 0.181	1.625 ± 0.341	0.515 ± 0.091
Quartzite	AL-04-G22	Pyrite containing quartzite	0.000656	0.288 ± 0.159	0.412 ± 0.268	0.144 ± 0.080

$\delta^{i}Fe = [(^{i}Fe/^{54}Fe)_{sample}/(^{i}Fe/^{54}Fe)_{IRMM014} - 1]^{*}10^{3}$, $F_{Fe} = \delta^{56}Fe/2$.
The compositions of metacarbonates IS-04-05 and IS-04-07 are given in Table 4.

absolute abundances than do LREEs. A similar feature had been observed by Frei and Jensen (2003) and Polat and Hofmann (2003) in Isua and had been attributed by these authors to greater susceptibility to metasomatic alteration of LREEs compared to HREEs. The mafic and ultramafic rocks from Akilia also show variable Eu/Eu* anomalies, ranging from 0.6 (SM/GR/97/3, Table 2) to 1.6 (AK03, Fedo and Whitehouse, 2002a) that may again reflect metasomatic alteration.

The REE patterns of undisputed BIFs from Isua with Fe/Ti > 1000 (all samples but one) are identical to the well-characterized geostandard IF-G (BIF from Isua, Govindaraju, 1994). These have concave upward curvatures ($La_N/Sm_N = 2.0–5.1$ and $Gd_N/Lu_N = 0.6–1.0$) with pronounced positive Eu/Eu* anomalies (1.3–2.5) and positive La/La* anomalies (1.2–1.4). The absolute concentrations

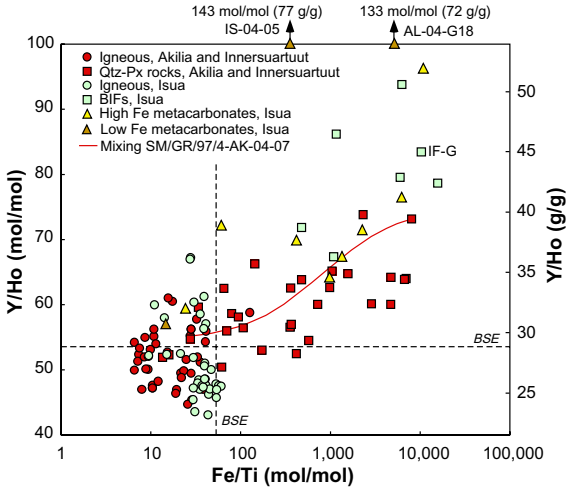

Fig. 7. Correlation between Y/Ho and Fe/Ti ratios in igneous rocks, metacarbonates, and rocks of inferred chemical sedimentary protoliths in Isua, Akilia, and Innersuartuut (data from Table 2; McGregor and Mason, 1977; Nutman et al., 1996; Fedo and Whitehouse, 2002a; Polat et al., 2002; Komiya et al., 2004; Cates and Mojzsis, 2006). The red curve is the trajectory for mixing between SM/GR/97/4 (gabbroic rock from Akilia; Dauphas et al., 2004a) and AK-04-07 (fine-grained Qtz-Px rock from Akilia, Table 2). The bulk silicate Earth composition (BSE) is from McDonough and Sun (1995). Two metacarbonates (IS-04-05 with Fe/Ti = 371 and Y/Ho = 143 and AL-04-G18 with Fe/Ti = 5407 and Y/Ho = 133; Table 2) plot off-scale on the Y/Ho axis. The right vertical axis gives the Y/Ho ratio in g/g (=0.539* mol/mol). (For interpretation of the references to color in this figure legend, the reader is referred to the web version of this paper.)

are lower than those of surrounding mafic and ultramafic rocks.

Except for sample IS-04-07, all metacarbonates from Isua with Fe/Ti > 1000 (IS-04-01, AL-04-G18, IS-04-02, and IS-04-10) have REE element patterns very similar to those of BIFs, with concave upward curvatures ($La_N/Sm_N = 1.3–6.2$ and $Gd_N/Lu_N = 0.4–1.6$), $Eu/Eu^* > 1$ (1.2–2.7) and $La/La^* > 1$ (1.1–1.8). The absolute REE concentrations ($0.9 < Sm_N < 8.3$) are also similar to those measured in BIFs ($0.54 < Sm_N < 2.72$). The metacarbonates with Fe/Ti < 1000 have typically higher REE concentrations and more variable patterns. Some of these rocks (e.g., IS-04-03, IS-04-09) have REE patterns that are reminiscent of those measured in mafic and ultramafic rocks (almost flat pattern with variable Eu/Eu*).

The REE element patterns of the Qtz-Px rocks from Akilia are variable with respect to absolute concentrations and the direction of Eu anomalies. Samples with Fe/Ti < 1000 tend to have higher concentrations (average $\text{Log } Sm_N = 1.01 \pm 0.39$, $n = 11$) than samples with Fe/Ti > 1000 (average $\text{Log } Sm_N = 0.25 \pm 0.34$, $n = 9$). The proportion of samples with $Eu/Eu^* > 1$ is higher in samples with Fe/Ti > 1000 (6 out of 9) compared to samples with Fe/Ti < 1000 (2 out of 11). Although some high Fe/Ti Qtz-Px rocks from Akilia share similarities with well-characterized BIFs from the ISB ($Eu/Eu^* > 1$, LREE enrichments), there are distinctive features between the two groups of samples. These include concave downward LREE patterns with low La/La* (average 0.89 ± 0.18 for Akilia $n = 9$, 1.29 ± 0.14 for Isua $n = 6$) and approximately flat HREE patterns (average Gd_N/Lu_N 1.14 ± 0.26 for Akilia $n = 8$, 0.78 ± 0.18 for Isua $n = 6$).

4.2. Iron isotopes in bulk rocks

Study of Qtz-Px rocks and metacarbonates suggests that trace elements were contaminated by addition of an igneous component, possibly through tectonic reworking or deposition of volcanic ashes. In the case of REE compositions of bulk rocks, we adopted a threshold of Fe/Ti > 1000 to try to distinguish between pristine and contaminated chemical sediments based on expected mixing trajectories (Fig. 7). In the case of the isotopic composition of a major element like Fe, a lower Fe/Ti threshold of 250 can be adopted because there is a very large contrast in Fe/Ti ratio between igneous rocks and metasomatic rocks/chemical sediments resulting in very high curvature of mixing trajectories (Fig. 9).

Table 4
Iron isotopic compositions of AC-E geostandard, carbonatites from the Kola Peninsula (Russia), and analytical tests done on metacarbonates from the ISB (southern West Greenland)

Type	Sample	Description	Fe (mol g^{-1})	δ^{56}Fe(‰)	δ^{57}Fe (‰)	F_{Fe} (‰/amu)
Granite	AC-E*[a]	Geostandard		0.268 ± 0.107	0.307 ± 0.156	0.134 ± 0.054
	AC-E III*[a]	Geostandard (three columns of AC-E*)		0.302 ± 0.107	0.442 ± 0.156	0.151 ± 0.054
	AC-E	Geostandard		0.275 ± 0.039	0.339 ± 0.051	0.137 ± 0.019
	AC-E	Geostandard		0.301 ± 0.038	0.400 ±0.172	0.151 ± 0.019
	AC-E	Geostandard		0.295 ± 0.067	0.414 ± 0.180	0.148 ± 0.034
	Average	AC-E	0.000316	0.289 ± 0.024	0.353 ± 0.044	0.144 ± 0.012
Carbonatite	NSB351-6	Kola carbonatite		−0.216 ± 0.098	−0.329 ± 0.151	−0.108 ± 0.049
	NSB351-6	Kola carbonatite		−0.345 ± 0.066	−0.505 ± 0.136	−0.173 ± 0.033
	NSB351-6	Kola carbonatite		−0.246 ± 0.100	−0.385 ± 0.131	−0.123 ± 0.050
	Average	NSB351-6		−0.291 ± 0.048	−0.411 ± 0.080	−0.146 ± 0.024
Carbonatite	BEG14	Kola carbonatite		−0.214 ± 0.067	−0.187 ± 0.179	−0.107 ± 0.034
	BEG14	Kola carbonatite		−0.260 ± 0.057	−0.415 ± 0.118	−0.130 ± 0.029
	Average	BEG 14		−0.241 ± 0.043	−0.346 ± 0.099	−0.120 ± 0.022
Reference	IRMM/IS-04-05*[a]	IRMM-014 in IS-04-05* matrix		−0.043 ± 0.139	−0.126 ± 0.269	−0.022 ± 0.070
Metacarbonate	IS-04-05*[a]	Carbonate w/ultramafics, W of the belt		−0.699 ± 0.162	−1.003 ± 0.312	−0.350 ± 0.081
	IS-04-05 III*[a]	Carbonate (three columns of IS-04-5*)		−0.754 ± 0.162	−1.140 ± 0.312	−0.377 ± 0.081
	IS-04-05	Carbonate		−0.752 ± 0.058	−1.098 ± 0.138	−0.376 ± 0.029
	IS-04-05	Carbonate		−0.724 ± 0.099	−1.106 ± 0.152	−0.362 ± 0.050
	Average	IS-04-05	0.000461	−0.742 ± 0.046	−1.096 ± 0.093	−0.371 ± 0.023
Reference	IRMM/IS-04-07*[a]	IRMM-014 in IS-04-07 matrix		0.020 ± 0.058	−0.056 ±0.120	0.010 ± 0.029
Metacarbonate	IS-04-07*[a]	Siderite, E of the belt		0.754 ± 0.058	1.110 ± 0.119	0.377 ± 0.029
	IS-04-07 III*[a]	Siderite (three columns of IS-04-07*)		0.783 ± 0.058	1.142 ± 0.120	0.392 ± 0.029
	IS-04-07	Siderite		0.705 ± 0.098	1.138 ± 0.154	0.353 ± 0.049
	Average	IS-04-07	0.01064	0.759 ± 0.038	1.129 ± 0.074	0.380 ± 0.019

[a] For some samples, the matrix was recovered from the first column. After getting rid of any Fe remaining from the sample by a second column, the matrix solution was doped with 100 μg of IRMM-014 Fe. Iron was extracted from this solution by two columns and its isotopic composition was analyzed (IRMM/IS-04-05* and IRMM/IS-04-07*). In parallel, iron that was eluted from the first column was further purified on a second column. At this stage, the solution was split into two aliquots. One measured directly by MC-ICPMS (AC-E*, IS-04-05*, and IS-04-07*) while the other was purified on a third column before analysis (AC-E III*, IS-04-05 III*, and IS-04-07 III*). $\delta^{i}Fe = [(^{i}Fe/^{54}Fe)_{sample}/(^{i}Fe/^{54}Fe)^{IRMM014} - 1] * 10^{3}$, $F_{Fe} = \delta^{56}Fe/2$.

The undisputed BIFs from Isua with Fe/Ti > 250 have heavy Fe isotopic compositions, ranging from +0.27 (9-1A2) to +0.51‰/amu (AL-6-2b). The samples have Ca/Fe, Mg/Fe, and Mn/Fe ratios (Fig. 10) similar to the extensively characterized BIF geostandard IF-G (0.0395, 0.0670, and 0.000846, respectively, Govindaraju, 1994). With high Ca/Fe, Mg/Fe, and Mn/Fe ratios compared to other BIFs, sample 10-1A2 is an outlier in terms of bulk chemistry but it has normal, heavy, Fe isotopic composition. All Qtz-Px rocks from Akilia measured in this study also have heavy Fe isotopic compositions relative to surrounding igneous rocks and IRMM-014 (from +0.190‰/amu AK-04-08 to +0.43‰/amu AK-04-07). These values are in the range documented by Dauphas et al. (2004a) for similar rocks sampled at the same locality (from +0.07 for AK-98 to +0.49‰/amu for G91-26). The Qtz-Px rocks from Akilia have significantly higher Ca/Fe, Mg/Fe, and Mn/Fe ratios than Isua BIFs, which may indicate formation of these rocks by decarbonation under granulite facies metamorphism (Manning et al., 2006; Nutman and Friend, 2006). Two samples taken at the interfaces between the Qtz-Px formation and surrounding mafic/ultramafic rocks have low Fe/Ti ratios and Fe isotopic compositions either similar to (AK-04-06 dark, southern contact, 0.000 ± 0.023‰/amu) or heavier than (AK-04-03 dark, northern contact, 0.152 ±0.043‰/amu) Eoarchean igneous rocks.

The major new finding of this study is the discovery of heavy and light Fe isotopic compositions (relative to IRMM-014) in metacarbonates from Isua (Tables 3 and 4). All metacarbonates rich in Fe (Mg-siderite) have heavy Fe isotopic compositions, ranging from +0.12 (IS-04-01) to +0.38‰/amu (IS-04-07). On average, Fe-rich metacarbonates have lower F_{Fe} values (+0.17 ± 0.13‰/amu, $n = 6$) compared to Isua BIFs (+0.37 ± 0.11‰/amu, $n = 7$) and Akilia/Innersuartuut Qtz-Px rocks (0.30 ± 0.15‰/amu, $n = 8$). The Fe isotope composition of AL-04-G22

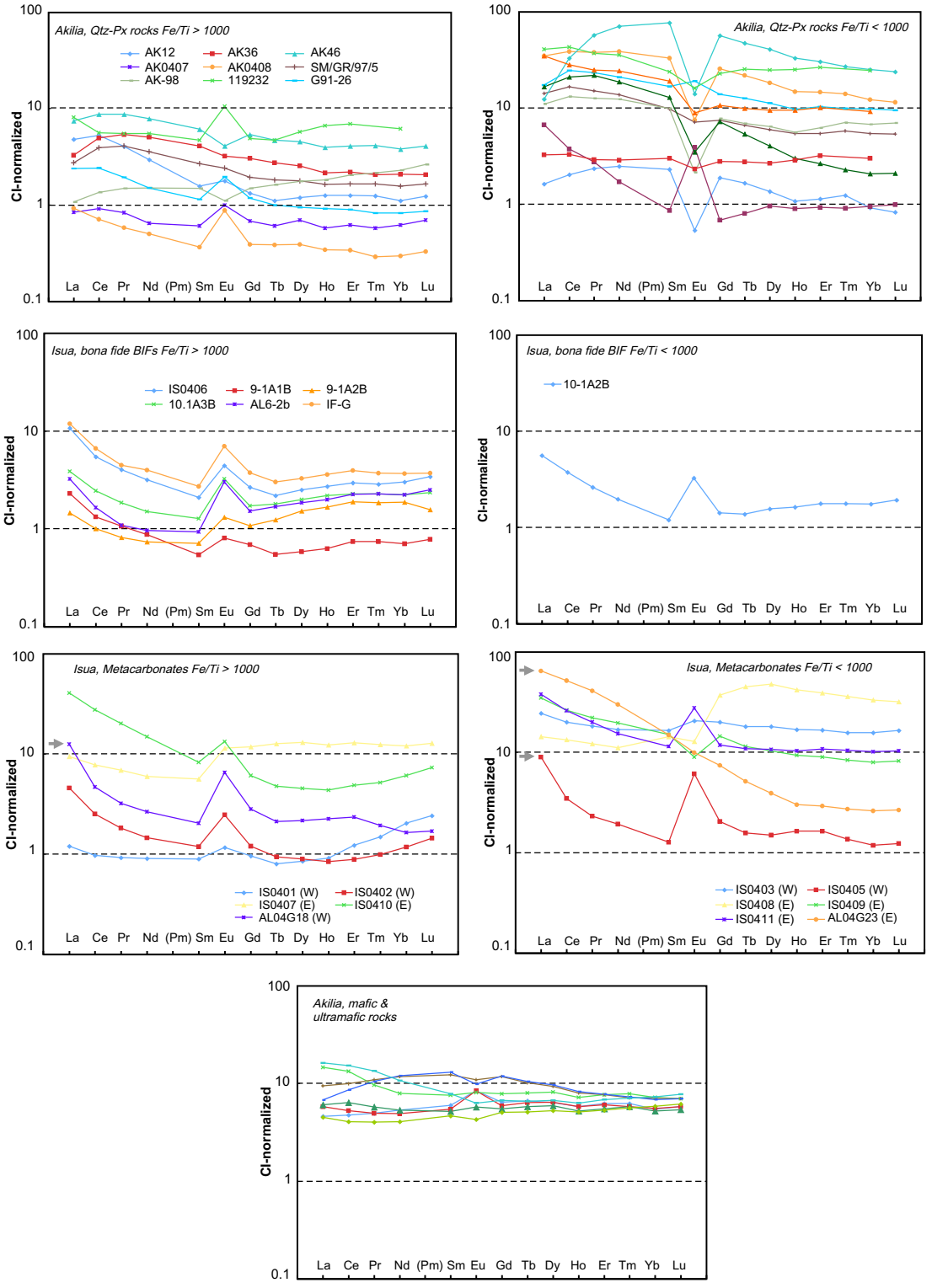

Fig. 8. Chondrite-normalized (Anders and Grevesse, 1989) REE patterns of Qtz-Px rocks from Akilia, igneous rocks from Akilia, BIFs from Isua, and metacarbonates from Isua. The Akilia Qtz-Px and Isua metacarbonate and BIF data were sorted into two groups each based on the Fe/Ti ratio (< or >10^3). The motivation for making such a distinction is based on Fig. 7 and the observation that for Fe/Ti ratios smaller than 10^3, trace element patterns may have been modified by mixing with an igneous component (Section 4.1). The metacarbonates with low Fe content and light Fe isotopic compositions (IS-04-05, AL-04-G18, and AL-04-G23) are marked with gray arrows. Data from Table 2; McGregor and Mason (1977); Nutman et al. (1996); Fedo and Whitehouse (2002a); Cates and Mojzsis (2006). For mafic and ultramafic rocks from Akilia, only those samples are plotted for which the whole suite of REEs (from La to Lu) have been analyzed (Table 2; Fedo and Whitehouse, 2002a).

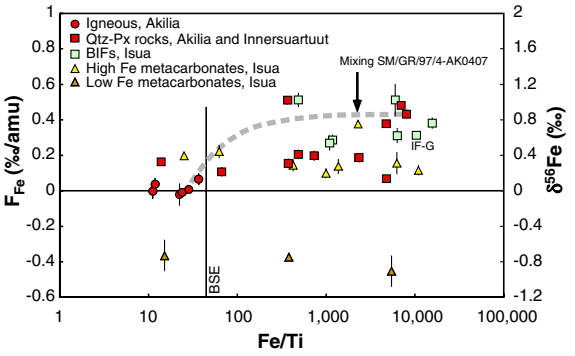

Fig. 9. Relationship between the Fe isotopic composition (expressed relative to IRMM-014) and the Fe/Ti ratio (Ti is an immobile element and the Fe/Ti ratio is a good proxy for Fe transport by fluids) in Eoarchean igneous rocks, metacarbonates, and rocks of inferred chemical sedimentary protoliths in Isua, Akilia, and Innersuartuut (data from Tables 2 and 3 and Dauphas et al., 2004a). The dashed gray line is the trajectory for mixing between SM/GR/97/4 (gabbroic rock from Akilia; Dauphas et al., 2004a) and AK-04-07 (fine-grained Qtz-Px rock from Akilia; Tables 2 and 3). The bulk silicate Earth composition (BSE) is from McDonough and Sun (1995).

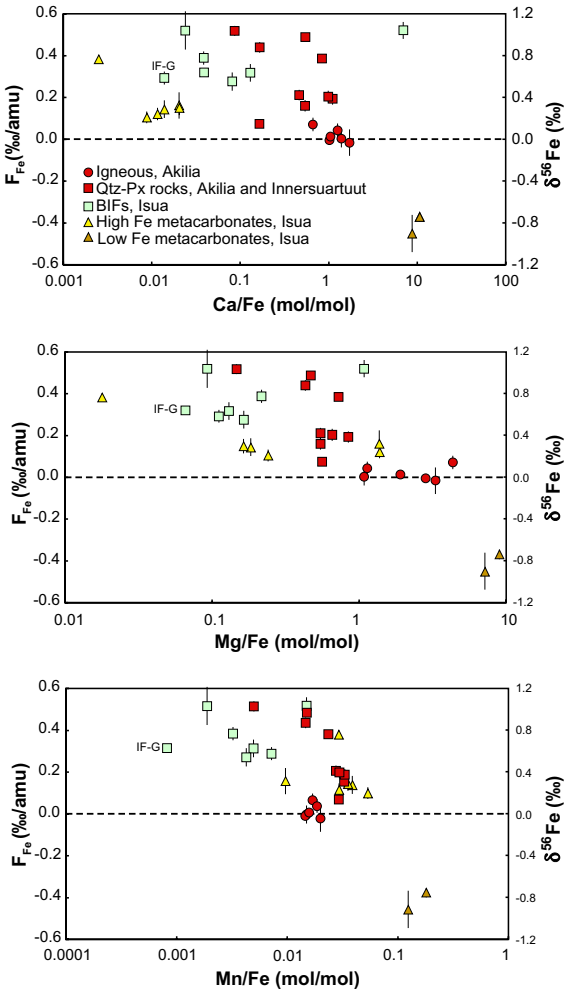

Fig. 10. Relationship between the Fe isotopic composition (relative to IRMM-014) and major element ratios (Ca/Fe, Mg/Fe, and Mn/Fe) for igneous and metasomatic/metasedimentary rocks from Isua and Akilia/Innersuartuut (Tables 2 and 3; note that for metasomatic/metasedimentary rocks, only samples with Fe/Ti > 250 were plotted, see Section 4.2 for explanations).

(Table 3), a quartzite in which pyrite is the principal carrier of Fe (Table 1), is similar to that documented in Fe-rich metacarbonates. The sample with the highest F_{Fe} value of all metacarbonates measured in this study (IS-04-07, +0.380‰/amu) also has the lowest Ca/Fe and Mg/Fe but has normal Mn/Fe. Fig. 11 compares the F_{Fe} values measured in Fe-rich metacarbonates from this study with data of other carbonates formed in a variety of conditions and geological settings (Table 4 for carbonatites; Johnson et al., 2003; Dideriksen et al., 2006; Markl et al., 2006; Frost et al., 2007). Regardless of their origin (magmatic, hydrothermal, metasomatic, or sedimentary) and age (Phanerozoic or Precambrian), carbonates usually have light Fe isotopic compositions relative to IRMM-014. The enrichment in heavy Fe isotopes observed in Fe-rich metacarbonates studied here is atypical.

4.3. Fe isotopes in individual minerals

Several pure mineral phases were sampled using a microdrilling apparatus and by hand-picking. Petrographic context and Fe isotope results are shown in Figs. 5 and 6 and in Table 5. Magnetite was sampled in nine different layers of a BIF from Isua (IS-04-06) over a distance of ~2 cm (Fig. 5). The Fe isotopic composition of magnetite is homogeneous at the scale of the section studied (MSWD = 1.39, within the two-sided 95% interval predicted from the reduced χ^2 distribution for $n-1=8$ degrees of freedom, 0.27–2.19). The weighted average F_{Fe} value of the nine individual magnetite analyses is 0.367 ± 0.026‰/amu. Two bulk measurements of IS-04-06 give a weighted average of 0.313 ± 0.042‰/amu. These two values are identical within error bars but magnetite seems to lie on the heavy side of the bulk composition. A similar feature has been observed by Dauphas et al. (2007) in BIFs from Nuvvuagittuq (Nothern Québec, Canada) metamorphosed under amphibolite facies. It could reflect small equilibrium fractionation at high temperature between magnetite and other carriers of Fe (i.e., heavy magnetite relative to carbonates, amphiboles, and the bulk rock).

Individual mineral phases were also analyzed in sample AL-44 (see Lepland et al., 2002; van Zuilen et al., 2003 for details). Microdrilling locations and Fe isotope results are shown in Fig. 6. In the following: Cbt, Gt, and Mgt are abbreviations for Mg-siderite carbonate $Mg_{0.48}Ca_{0.01}Mn_{0.07}Fe_{0.44}CO_3$, Almandine garnet ($Fe_{2.14}Mn_{0.56}Mg_{0.24}Ca_{0.06}$)$Al_2Si_3O_{12}$, and magnetite Fe_3O_4 fractions, respectively. In siderite and almandine, iron is present as Fe^{2+} while in magnetite it is present as both Fe^{2+} and Fe^{3+} in a ratio 1:2. Imaging and X-ray analysis by SEM allowed us to quantify the purity of each separated phase (Cbt1: 100% Cbt; Cbt2: 94% Cbt and 6% Mgt; Cbt3: 97% Cbt, 1% Gt, and 2% Mgt; Gt1: 100% Gt; Gt2: 12% Cbt and 88% Gt; Gt3: 100% Gt; Mgt1, Mgt2, and Mgt3: 100% Mgt, where the percentages correspond approximately to

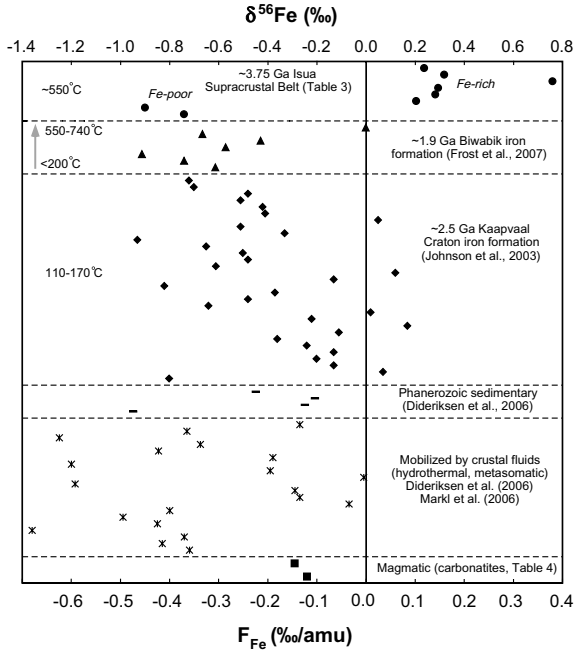

Fig. 11. Comparison between the Fe isotopic composition of metacarbonates from the ISB (top panel, Tables 3 and 4) and carbonates formed in a variety of geological settings (Table 4 for carbonatites; Johnson et al., 2003; Dideriksen et al., 2006; Markl et al., 2006; Frost et al., 2007). Note that for Isua metacarbonates, only samples with Fe/Ti > 250 are shown (see Section 4.2 for explanations). While most carbonates analyzed until now and Fe-poor carbonates from Isua have negative F_{Fe} values, Fe-rich carbonates show consistently positive F_{Fe} values.

volume fractions). All carbonate separates (Cbt1, 2, and 3) have identical Fe isotopic compositions within error, averaging -0.042 ± 0.024‰/amu. Two garnet analyses give identical compositions ($+0.008 \pm 0.052$ and -0.027 ± 0.038‰/amu for Gt1 and Gt3, respectively) relative to each other and the carbonate fractions. Gt2 has a lower F_{Fe} value of -0.159 ± 0.052‰/amu. At this stage, we have no clear explanation for that. Gt2 contains the largest amount of impurity of all the fractions studied (12% carbonate) but given the measured composition of the Cbt fractions, this cannot explain the low F_{Fe} value measured in Gt2. The most likely reason is that garnet is not at equilibrium at the scale of the section studied. All three magnetite analyses are enriched in the heavy Fe isotopes relative to carbonates and garnets. The weighted average F_{Fe} value of Mgt1, Mgt2, and Mgt3 is $+0.148 \pm 0.026$‰/amu. The rocks studied were metamorphosed under regional amphibolite facies metamorphism. The difference in Fe isotopic composition between (i) magnetite and Mg-siderite and (ii) magnetite and almandine (with Gt2 excluded) are $+0.190 \pm 0.036$ and $+0.163 \pm 0.040$‰/amu, respectively ($+0.379 \pm 0.071$ and $+0.325 \pm 0.081$‰ for δ^{56}Fe).

Some of the metacarbonates (e.g., IS-04-01, IS-04-02, and IS-04-03) have been extensively weathered after denudation and during exposure at the surface. A large fraction of siderite was converted into Fe-oxyhydroxide (Table 1). To address the question of whether or not such weathering affected the Fe isotopic composition of the bulk rock, we analyzed the composition of mineral phases that are not prone to weathering (magnetite when available or amphibole/chlorite, Table 5). All mineral separates have Fe isotopic compositions that are similar to or higher than the bulk analyses. Using mineral mode analysis (Table 1) and equilibrium fractionation between mineral phases at closure temperature (~400–600 °C), it is possible to calculate a bulk Fe isotopic composition before weathering (it is assumed that all Fe in Fe-oxyhydroxide was initially in siderite and that the rock behaved as a closed system for Fe). For simplicity, we adopt magnetite-carbonate and magnetite-silicate fractionations of ~0.15–0.35‰/amu (magnetite–siderite and magnetite–hedenbergite equilibrium fractionations from Polyakov and Mineev, 2000; Polyakov et al., 2007). For most samples, the computed pre-weathering bulk compositions obtained from magnetite or amphibole analyses agree with direct bulk measurements (Fig. 12). Two out of eight samples fall above the 1:1 correlation and this may be due to a lower closure temperature (larger inter-mineral fractionation) than that adopted here and/or non closed-system behavior. Thus, the heavy Fe isotopic compositions measured in metacarbonates cannot be explained by weathering.

5. DISCUSSION

5.1. The Fe isotopic composition of Eoarchean seawater

The processes that may be responsible for the Fe isotope and trace element compositions measured in BIFs have been discussed extensively in literature and will be discussed only briefly here. BIFs are chemical precipitates that formed early in Earth's history, before the atmosphere and ocean became oxic. One major issue in understanding the formation of these rocks is identifying the mechanism responsible for Fe-oxidation and precipitation in a globally anoxic atmosphere. Three mechanisms have been suggested (i) photo-oxidation by energetic UV photons (Braterman et al., 1983); (ii) oxidation by O_2 released by oxygenic photosynthesis (Cloud, 1983), possibly auto-catalyzed by the presence of ferric-(hydr)oxide (Dauphas et al., 2007); and (iii) direct oxidation by anoxygenic photosynthetic bacteria (Widdel et al., 1993). The source of Fe in the Archean ocean is thought to be hydrothermal.

Our results confirm the observation of Dauphas et al. (2004a) that BIFs from Isua have heavy Fe isotopic compositions relative to IRMM-014. For comparison, Fe-oxides in BIFs from other localities show similar signatures (Johnson et al., 2003; Rouxel et al., 2005; Dauphas et al., 2007; Frost et al., 2007). An important observation is that in weakly metamorphosed BIFs, different minerals have different Fe isotopic compositions (sulfides and carbonates tend to be isotopically light while oxides tend to be isotopically heavy, Johnson et al., 2003; Rouxel et al., 2005; Frost et al., 2007). Modern hydrothermal systems release Fe with light isotopic composition relative to IRMM-014, around −0.15‰/amu (Sharma et al., 2001; Beard et al., 2003a; Severmann et al., 2004). The most likely reason for the enrichment in the heavy isotopes of Fe in BIFs from Isua relative

Table 5
Microdrill and mineral separate analyses of BIFs and metacarbonates from the ISB (southern West Greenland)

Type	Sample	Description[a]	δ^{56}Fe (‰)	δ^{57}Fe (‰)	F_{Fe} (‰/amu)
Microdrilled mineral, IS-04-06	IS1S1	Magnetite (2.1)	0.744 ± 0.164	1.111 ± 0.295	0.372 ± 0.082
	IS3S1	Magnetite (1.7)	0.859 ± 0.164	1.262 ± 0.295	0.430 ± 0.082
	IS4S1	Magnetite (1.15)	0.655 ± 0.164	0.885 ± 0.295	0.328 ± 0.082
	IS6S1	Magnetite (0.85)	0.819 ± 0.164	1.139 ± 0.295	0.410 ± 0.082
	IS7S1	Magnetite (0.75)	0.731 ± 0.164	1.081 ± 0.295	0.366 ± 0.082
	IS8S1	Magnetite (0.6)	0.618 ± 0.164	0.944 ± 0.295	0.309 ± 0.082
	IS9S1	Magnetite (0.2)	0.629 ± 0.164	0.938 ± 0.295	0.315 ± 0.082
	IS10S1	Magnetite (0.15)	0.874 ± 0.164	1.283 ± 0.295	0.437 ± 0.082
	IS11S1	Magnetite (0.1)	0.706 ± 0.116	1.035 ± 0.209	0.353 ± 0.058
Microdrilled mineral, AL-44	Cbt1	Mg-siderite	−0.082 ± 0.104	−0.167 ± 0.134	−0.041 ± 0.052
	Cbt2	Mg-siderite	−0.080 ± 0.076	−0.115 ± 0.118	−0.040 ± 0.038
	Cbt3	Mg-siderite	−0.089 ± 0.076	−0.123 ± 0.118	−0.045 ± 0.038
	Gt1	Almandine	0.015 ± 0.104	0.018 ± 0.134	0.008 ± 0.052
	Gt2	Almandine	−0.317 ± 0.104	−0.483 ± 0.134	−0.159 ± 0.052
	Gt3	Almandine	−0.054 ± 0.076	0.104 ± 0.118	−0.027 ± 0.038
	Mgt1	Magnetite	0.181 ± 0.104	0.295 ± 0.134	0.091 ± 0.052
	Mgt2	Magnetite	0.335 ± 0.104	0.473 ± 0.134	0.168 ± 0.052
	Mgt3	Magnetite	0.335 ± 0.076	0.524 ± 0.118	0.168 ± 0.038
Handpicked mineral	IS-04-01-mgt	Magnetite	0.921 ± 0.193	1.292 ± 0.240	0.460 ± 0.097
	IS-04-02-amp	Amphibole + chlorite	0.791 ± 0.170	1.162 ± 0.263	0.396 ± 0.085
	IS-04-03-amp	Amphibole + chlorite	0.436 ± 0.170	0.658 ± 0.263	0.218 ± 0.085
	IS-04-07-mgt	Magnetite	0.891 ± 0.158	1.296 ± 0.196	0.446 ± 0.079
	IS-04-08-mgt	Magnetite	0.935 ± 0.193	1.317 ± 0.240	0.468 ± 0.097
	IS-04-09-mgt	Magnetite	0.349 ± 0.158	0.543 ± 0.196	0.174 ± 0.079
	IS-04-10-mgt	Magnetite	0.660 ± 0.223	0.959 ± 0.277	0.330 ± 0.111
	IS-04-11-mgt	Magnetite	0.645 ± 0.173	0.860 ± 0.215	0.323 ± 0.086

$\delta^{i}Fe = [(^{i}Fe/^{54}Fe)_{sample}/(^{i}Fe/^{54}Fe)_{IRMM014} - 1] * 10^{3}$, $F_{Fe} = \delta^{56}Fe/2$.
[a] The numbers in parentheses are the distances in centimeters from the bottom of the sample in Fig. 5.

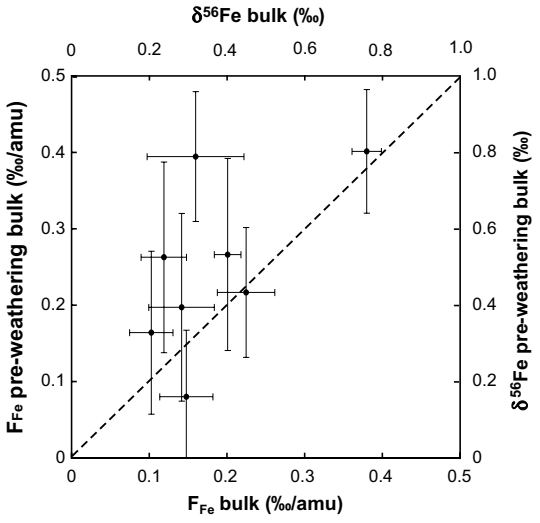

Fig. 12. Comparison between bulk metacarbonate Fe isotopic composition and pre-weathering bulk composition estimated from mineral separate analyses. Some metacarbonates have been extensively weathered. In particular, siderite was converted into Fe-oxyhydroxide. Magnetite and amphiboles/chlorite are less prone to weathering. Using the Fe isotopic composition of individual minerals (Table 5), the mineral mode analysis (Table 1), and estimated inter-mineral fractionations at 450–650 °C (Section 4.3), it is possible to calculate a pre-weathering bulk composition.

to the hypothetical source fluid (hydrothermal) is partial oxidation of $Fe(II)_{aq}$ in the water column (Dauphas et al., 2004a). Indeed, all oxidation mechanisms documented so far tend to enrich the product in the heavy isotopes of Fe by 0.5–1.7‰/amu (Bullen et al., 2001; Welch et al., 2003; Croal et al., 2004; Balci et al., 2006). Two chemical pathways that have not been explored yet for Fe isotopic fractionation are heterogeneous oxidation (Tamura et al., 1976) and photo-oxidation (Braterman et al., 1983). The net isotope fractionation between $Fe(II)_{aq}$ and $Fe(III)_s$ can be modulated by kinetic isotope fractionation at precipitation, which tends to enrich the solid in the light isotopes of Fe and hence counteract the effect of partial oxidation (Skulan et al., 2002). At very high precipitation rate, supply of Fe to the growing phase becomes limited by diffusion in the fluid and Fe(III)s has the same isotopic composition as $Fe(II)_{aq}$ (Dauphas and Rouxel, 2006). Regardless of these complications, the heavy Fe isotopic composition of BIFs from Isua (+0.35‰/amu) is best explained by partial oxidation in a marine setting ($\Delta = 0.5$–1.7‰/amu) of a hydrothermal source with Fe isotopic composition around −0.15‰/amu. At this stage, Fe isotopes cannot discriminate between the different oxidation mechanisms.

Another possible interpretation would be that the source fluid of BIFs from Isua had heavy Fe isotopic composition and that this signature was transferred into sediments without isotopic fractionation upon precipitation. Several arguments speak against such a scenario. Johnson et al. (2003)

analyzed mineral separates in ~2.5 Ga BIFs from the Kaapvaal Craton. The rocks were heated only to 110–170 °C and the isotopic variations measured in minerals reflect, albeit with diagenetic and subtle metamorphic modifications, the conditions of deposition. Assuming equilibrium conditions and using available β-factors for $Fe(II)_{aq}$, $Fe(III)_{aq}$, siderite, ankerite, magnetite, and hematite, they were able to estimate the composition of the source fluid and concluded that "*although the uncertainties in the preferred set of β factors remains significant, the calculations are suggestive that the Fe(II) species that were associated with BIF formation had* δ^{56}*Fe values that were less than zero, consistent with a MOR-hydrothermal source*".

Rouxel et al. (2005) measured the Fe isotopic composition of sedimentary pyrite covering a time span (2.7 Ga to present) that encompasses the rise of atmospheric O_2 at around 2.3 Ga. They found that pyrite formed before 2.3 Ga had variable, predominantly negative F_{Fe} values (down to −1.7‰/amu) while pyrite formed after ~1.7 Ga had F_{Fe} values similar to detrital sources (~0‰/amu). They argued that the negative F_{Fe} values of >2.3 Ga pyrite reflect variations in the F_{Fe} value of seawater. In this context, partial oxidation associated with BIF precipitation would have left a residue of isotopically light $Fe(II)_{aq}$ (<−0.15‰/amu). Yamaguchi and Ohmoto (2006) and Archer and Vance (2006) questioned this interpretation and suggested instead that the light Fe isotopic compositions measured in >2.3 Ga pyrite grains reflect microbial cycling of Fe in the sediment by dissimilatory iron reduction (however, see Rouxel et al., 2006). Studies of shallow sediment profiles (Severmann et al., 2006; Staubwasser et al., 2006) have shown that such redox cycling does occur in present-day sediments, producing $Fe(II)_{aq}$ in porewaters with F_{Fe} as low as −1.5‰/amu.

Dauphas et al. (2007) measured the Fe isotopic composition in >3.75 Ga BIFs from Nuvvuagittuq (Northen Québec, Canada). A relationship between Ca/Fe, Mg/Fe, and Mn/Fe ratios and F_{Fe} values defined by two clusters of points (not seen here, as is evident from Fig. 10) was interpreted to reflect mixing between primary carbonates and Fe-(hydr)oxides in the sediment before metamorphism. Using this relationship, Dauphas et al. (2007) showed that the primary carbonates and the precursor of magnetite had negative and positive F_{Fe} values, respectively. This is reminiscent of what was observed in more recent and better preserved BIFs (Johnson et al., 2003; Frost et al., 2007) and is consistent with derivation of these >3.75 Ga BIFs from a marine hydrothermal source.

At this stage, there is no reason to doubt that the main inventory of Fe in the Eoarchean ocean had an isotopic composition similar to or lighter than IRMM-014 and that the positive F_{Fe} values measured in BIFs from Isua reflect partial oxidation of ferrous Fe emanating from MOR-type hydrothermal vents.

5.2. Metacarbonates

The interpretation of carbonate rocks found in the ISB is complicated by metasomatic processes. Identifications in different studies range from a pure sedimentary to a pure metasomatic origin. Iron-rich metacarbonates in the belt were initially described as carbonate-facies iron formations, deposited as chemical sediments in a marine setting (Schidlowski et al., 1979; Appel, 1980, 1983; Nutman et al., 1984; Dymek and Klein, 1988; Shimizu et al., 1990; Mojzsis et al., 1996). Rose et al. (1996) and Rosing et al. (1996) called this idea into question and proposed instead a metasomatic origin for the metacarbonates. van Zuilen et al. (2002, 2003) showed that the magnetite found in siderite-rich lithologies was formed by thermal decomposition at a temperature of >450 °C following the reaction, $6FeCO_3 \rightarrow 2Fe_3O_4 + 5CO_2 + C$ (Perry and Ahmad, 1977). More recently, Bolhar et al. (2004) measured the REE + Y pattern of a magnetite-bearing carbonate and suggested that it was typical of a seawater precipitate and therefore that the rock was sedimentary in origin. Determining which carbonates are sedimentary or metasomatic in origin is important. Indeed, for those that represent primary chemical precipitates, the presence of siderite would indicate deposition under high pCO_2 (Rye et al., 1995; Ohmoto et al., 2004). This is significant since CO_2 is a greenhouse gas that could have compensated for lower solar luminosity in the early Archean (e.g., Owen et al., 1979; Kasting, 1987). If formed by DIR, this would indicate that this metabolic pathway (e.g., Lovley, 1991) had already developed by ~3.8 Ga. The question of the nature of the metacarbonates is also relevant to studies of the earliest traces of life (e.g., Mojzsis et al., 1996; van Zuilen et al., 2002, 2003).

The origin of carbonates found in Isua can be addressed using REE abundances and Fe isotope compositions. In Isua, all studied metacarbonates with Fe/Ti > 1000 except IS-04-07 show trace element characteristics that are generally considered typical for seawater derivation as described by Bolhar et al. (2004) and Frei and Polat (2007). Samples AL-04-G18 and IS-04-05 (Fe-poor carbonates from location 1 in the western part of the belt) have similar REE patterns, but the Y/Ho ratios of these samples are extremely high. Interestingly, Rose et al. (1996) and Rosing et al. (1996) took replacive carbonates from this location as case examples of metasomatic derivation (see Section 2.1 for a brief outline of their model). Bau (1996) showed that the Y/Ho ratio of hydrothermal carbonates could be elevated. At present, it is unclear to what extent metasomatic rocks can mimic some features of chemical sediments. On the basis of REE + Y alone, one cannot rule out a metasomatic origin for the rocks studied by Rose et al. (1996) and Rosing et al. (1996) as well as the metacarbonate samples studied here, especially when that contradicts with field and petrographic evidence.

Iron isotopes can provide useful constraints on the origin of the metacarbonates. In the metasomatic scenario, Fe is derived from leaching of preexisting protoliths. Basalt alteration in the oceanic crust tends to leave a residue that is enriched in the heavy isotopes of Fe, so the fluid must become light compared to the source rock (Rouxel et al., 2003). The isotopic composition of Fe dissolved from hornblende in laboratory-controlled experiments at room temperature is identical or lighter compared to the source mineral (Brantley et al., 2001, 2004). Leaching of Fe from rocks is a complex process that is to some extent kinetically

controlled and it is impossible to accurately predict what the isotopic composition of dissolved Fe would be. Given the high temperature involved (550 °C), the absence of changes in the redox state of Fe (2+), and available evidence from natural analogues and laboratory experiments (Brantley et al., 2001, 2004; Rouxel et al., 2003), it is reasonable to assume that Fe leached from ultramafic rocks would have zero or negative F_{Fe} values. Contrary to mineral dissolution, which is to some degree kinetically controlled, isotopic fractionation during mineral precipitation can be safely described using equilibrium fractionation factors. One can calculate the siderite–$Fe(H)_2O_6^{2+}$ equilibrium fractionation using the β-values of Polyakov and Mineev (2000) for siderite and those of Anbar et al. (2005) for $Fe(II)_{aq}$. The DFT-PCM theoretical predictions of Anbar et al. (2005) only extend to 300 °C but at all temperatures, siderite is expected to have light Fe isotopic composition relative to $Fe(II)_{aq}$ and if one were to extrapolate the fractionation as a function of $1/T^2$ to a temperature of 550 °C, the siderite-$Fe(II)_{aq}$ would only be −0.2‰/amu. The isotopic fractionation may have been even lower if Fe(II) speciation in the fluid was dominated by carbonate complexes. Overall, it is likely that siderite formed metasomatically from leaching of ultramafic rocks would have a light Fe isotopic composition relative to the source.

The samples of location 1 (Fig. 1) represent the type of metacarbonate that was described by Rose et al. (1996). These rocks are closely associated with ultramafic bodies, and have a clear replacive character (Fig. 3a–c). Actinolite and tremolite in these samples are interpreted as products of a metamorphic reaction between quartz and carbonate. All three samples have negative F_{Fe} values (−0.4‰/amu on average), which is in line with (but does not unambiguously demonstrate) leaching of Fe from an igneous source and subsequent deposition as a carbonate phase.

In contrast to location 1, metacarbonates from locations 2 and 3 show heavy Fe isotopic compositions relative to IRMM-014 and surrounding igneous rocks. Carbonates typically have light Fe isotopic compositions, whether they are formed by sedimentary, diagenetic, or metamorphic processes (Fig. 11 and Table 4; Johnson et al., 2003; Dideriksen et al., 2006; Markl et al., 2006; Frost et al., 2007). The heavy Fe isotopic compositions measured in Fe-rich metacarbonates from Isua are inconsistent with an ultramafic source of Fe.

A possible interpretation for the heavy isotopic composition of Fe-rich metacarbonates is that they were formed as chemical sediments. This interpretation appears consistent with similarities observed in the REE + Y composition of Isua BIFs and Fe-rich metacarbonates with elevated Fe/Ti. A question in an entirely sedimentary scenario remains however: how did carbonates inherit positive Fe isotope signatures which are thought to be produced by partial oxidation of $Fe(II)_{aq}$ dissolved in seawater? One possibility is that magnetite present in these metacarbonates was not formed by disproportionation of siderite but instead was derived from transformation of a hydrous ferric oxide precursor. Speaking against this idea is the lack of correlation between the Fe isotopic composition and the fraction of Fe locked up in magnetite (Fig. 13). A second possibility in the sedimentary scenario may be that a hydrous ferric oxide precursor was transformed into Fe-bearing carbonate during diagenesis, possibly promoted by the activity of bacteria that carry out dissimilatory iron reduction (DIR). This mechanism would imply a relationship between produced carbonate and organic matter (graphite), which is not observed. Instead the graphite abundance correlates with magnetite, consistent with graphite and magnetite formation through siderite decomposition (Lepland et al., 2002; van Zuilen et al., 2002, 2003). Another difficulty with this scenario is that during DIR, the pool of $Fe(II)_{aq}$ from which siderite could form tends to be enriched in the light isotopes of Fe relative to starting ferric-(hydr)oxide (Beard et al., 1999, 2003b; Icopini et al., 2004; Johnson et al., 2005; Crosby et al., 2005, 2007).

The most likely interpretation is that Fe in Fe-rich metacarbonates (and a pyrite-chert) originates from leaching of a BIF precursor by metasomatic fluids. This is consistent with independent geochemical and field evidence for metasomatism at locations 2 and 3 (Lepland et al., 2002; van Zuilen et al., 2003, 2005).

5.3. The origin of Qtz-Px rocks in Akilia

The origin of the banded Qtz-Px unit found on Akilia Island has been the subject of much debate over the past 10 years (see Sections 1 and 2). Some argued that these rocks were formed by precipitation in seawater (McGregor and Mason, 1977; Mojzsis et al., 1996; Nutman et al., 1997; Friend et al., 2002; Mojzsis and Harrison, 2002; Palin, 2002; Dauphas et al., 2004a; Manning et al., 2006; Nutman and Friend, 2006) while others advocated a metasomatic origin whereby quartz infiltration and deformation would have resulted in a rock that superficially mimics a metasediment (Fedo and Whitehouse, 2002a,b,c; Bolhar et al., 2004;

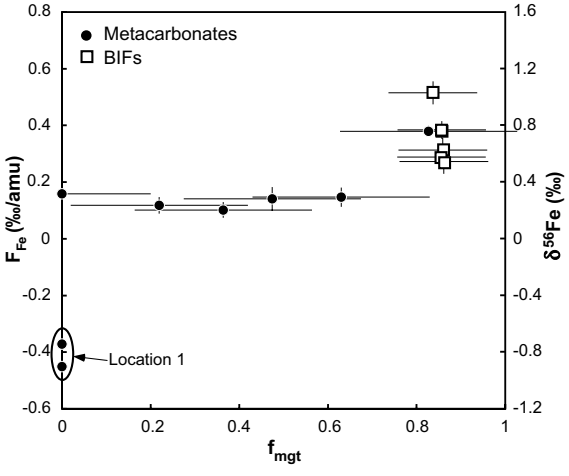

Fig. 13. Relationship between the Fe isotopic composition (‰/amu relative to IRMM-014, Table 3) and the fraction of the total Fe present in the sample as magnetite (f_{mgt} calculated from the mineral modes presented in Table 1) in metacarbonates and BIFs from the ISB (only samples with Fe/Ti > 250 are plotted here; see Section 4.2).

André et al., 2006; Fedo et al., 2006). The recent studies of Dauphas et al. (2004a) and Manning et al. (2006) provide additional evidence that the rocks have a chemical sedimentary protolith. We confirm the conclusions of Dauphas et al. (2004a) that the Qtz-Px rocks from Akilia are markedly enriched in the heavy isotopes of Fe compared with surrounding igneous rocks (Fig. 9). This is best explained by oxidation and subsequent precipitation of Fe in a marine setting. The Qtz-Px rocks from Akilia contain little magnetite so the ferric-(hydr)oxide carrier of heavy Fe must have been reduced at some stage, including possibly during diagenesis or incipient metamorphism.

Dauphas et al. (2004a) used Fe/Ti ratios (together with Fe isotopes) to argue for a chemical sedimentary origin of Qtz-Px rocks found in Akilia because seawater contains little Ti and this feature is transferred to the chemical sediment at precipitation. Polat and Hofmann (2003) studied alteration of trace element patterns of igneous rocks in Isua by metamorphism–metasomatism associated with shear zones and concluded that Ti was less mobile than most other elements, including LREEs. Fedo et al. (2006) questioned the validity of using Ti as an anchor because it can be transported at the meter scale in deep crustal shear zones but the same authors used LREEs to infer the nature of the protolith of Qtz-Px rocks from Akilia, with the underlying assumption that these elements are immobile. Even if Ti was partly mobile, this cannot explain the variations over three orders of magnitude for Fe/Ti ratios documented in Akilia (O'Hara and Blackburn, 1989; Ague, 1991; Dauphas et al., 2004a).

We recognize that there are still difficulties with the sedimentary interpretation. As discussed by Bolhar et al. (2004), the REE + Y patterns of several Akilia Qtz-Px rocks are variable and distinct from Isua BIFs (Fig. 8, Section 4.1). Friend et al. (2002) and Nutman and Friend (2006), noted however that only the finest grained, most magnetite-rich part of the Qtz-Px formation has a trace element pattern very similar to typical BIFs from Isua, so sampling might be critical. There is general agreement that Eu/Eu* anomalies are easily modified during high grade metamorphism and do not provide an unambiguous test for or against seawater derivation (e.g., Fedo and Whitehouse, 2002a; Bolhar et al., 2004; Manning et al., 2006). Still, the proportion of Qtz-Px rocks with Eu/Eu$^* > 1$ is higher among the samples with Fe/Ti > 1000 (6/9) compared to samples with Fe/Ti < 1000 (2/11). The lack of positive La anomaly in Akilia is more troublesome for a sedimentary interpretation (Isua BIFs have La/La$^* > 1$ while most Qtz-Px rocks with Fe/Ti > 1000 have La/La$^* < 1$). However, in modern oceans, this feature is controlled by solution complexation/surface complexation during particle scavenging (Byrne and Kim, 1990; Bau, 1999; Quinn et al., 2004; Section 4.1) and there is no a priori reason to expect that the source of Fe in Akilia went through the same history of scavenging as BIFs from Isua if these two formations formed at slightly different times or environment (Akilia supracrustals could be ~100 My younger or older than the ISB, e.g., Nutman et al., 1997; Whitehouse et al., 1999; Manning et al., 2006). In the modern ocean, the residence time of trivalent REEs is lower than the mixing timescale (~1.5 ky) so that heterogenous εNd (Piepgras et al., 1979; Elderfield, 1988) and REE patterns (Zhang et al., 1994; Bau, 1996; Nozaki et al., 1997) are found in different ocean basins. The REE composition is also expected to change with time. This could also explain why the Y/Ho ratio of Akilia Qtz-Px rocks with Fe/Ti > 1000 is superchondritic (35–40 g/g) but still lower than that found in Isua BIFs (40–50 g/g). In the modern ocean, this ratio varies between ~40–70 g/g (Bau, 1996). To summarize, Fe isotopes are best explained if the banded Qtz-Px rocks from Akilia have a sedimentary origin.

5.4. Magnetite–siderite and magnetite-pyroxene Fe isotope thermometry

Using Mössbauer spectroscopic data, Polyakov and Mineev (2000) calculated the iron reduced isotopic partition function ratios (β-factors) and their variations with temperature for a variety of minerals. They concluded that the β-factors of Fe^{3+} ions are considerably higher than those of Fe^{2+} and identified the mineral pair magnetite–siderite as a potential geothermometer. Recently, Polyakov et al. (2007) revised the β-factors for siderite and magnetite using Inelastic Nuclear Resonance X-ray Scattering (INRXS) corresponding to an updated equation for fractionation between magnetite and siderite,

$$\Delta Fe_{magnetite-siderite} = 0.13399x - 1.2668 \times 10^{-3}x^2 + 0.54997 \times 10^{-6}x^3 \ (‰/amu) \quad (1)$$

where $x = 10^6/T^2$ with T the absolute temperature in degrees Kelvin (K). Frost et al. (2007) measured adjacent carbonates and magnetite in the contact metamorphosed Biwabik iron formation, Minnesota, USA. The rocks were heated to peak temperatures ranging from < 200 to 550–740 °C. Frost et al. (2007) found variations in the Fe isotopic compositions of carbonates and magnetite that do not conform to INRXS predictions. As discussed by these authors, the reason is that even at the highest grade, magnetite did not equilibrate with other phases. Part of the variations must therefore have been inherited from fractionation during deposition and low-grade metamorphism (Johnson et al., 2003). Contrary to the contact metamorphosed Biwabik iron formation, Isua supracrustal rocks were regionally metamorphosed (amphibolite to granulite-facies). Such high grade regional metamorphism is expected to promote inter-mineral equilibration. Thus, these rocks may be appropriate for calibration of Fe isotope geothermometry. Another virtue of Isua is that a wide range of mineral assemblages is available (e.g., pyroxenes, amphiboles, carbonates, sulfides, garnets).

As discussed in Section 4.3, the isotopic fractionation measured between magnetite and Mg-siderite in sample AL-44 is $+0.190 \pm 0.036$‰/amu. van Zuilen et al. (2002, 2003) suggested that in AL-44, magnetite and graphite formed by thermal decomposition of siderite at >450 °C following the reaction $6FeCO_3 \rightarrow 2Fe_3O_4 + 5CO_2 + C$ (Fig. 6 shows the petrography of this sample). The three carbonate and three magnetite fractions from AL-44 have homogeneous Fe isotopic compositions. This supports the idea that Mg-siderite and magnetite in

AL-44 are in isotopic equilibrium. Boak and Dymek (1982) estimated a temperature of ~550 °C for the main stage of regional metamorphism in Isua. AL-44 was sampled in the Western part of the belt (Lepland et al., 2002), in domain IV of Rollinson, 2002). This domain was affected by 2–3 major episodes of metamorphism in the early (~3.74 Ga, Frei and Rosing, 2001) and late (~2.8 Ga, Grau et al., 1996; Frei et al., 1999) Archean. The temperatures for the early and late Archean events calculated based on garnet-biotite thermometry are ~610 and 550–570 °C, respectively (Rollinson, 2002). Because the temperatures are similar, the polyphase thermal history of the rock is not a problem for calibrating the siderite-magnetite thermometer on AL-44.

In Fig. 14a, we compare the magnetite–siderite Fe isotopic fractionation predicted by theory with the measured value in AL-44. At 550 °C, Polyakov and Mineev (2000) predict $\Delta Fe_{magnetite-siderite} = 0.41‰/amu$ based on Mössbauer spectra while the more recent estimate of Polyakov et al. (2007) based on INRXS gives a lower value of 0.19‰/amu. The value that is measured here is $+0.190 \pm 0.036‰/amu$. This result supports the use of Eq. (1) (Polyakov and Mineev, 2000; Polyakov et al., 2007) for Fe isotope fractionation between magnetite and siderite. We confirm the conclusion of Johnson et al. (2003) who noted that the β-factor of magnetite estimated by Polyakov and Mineev (2000) may be inaccurate. This value has now been superseded by a more recent estimate (Polyakov et al., 2007), which is in agreement with measured isotopic fractionations in natural samples. As discussed by Polyakov et al. (2007), the difference between the two estimates is due to improvement in the input data.

Dauphas et al. (2004a) separated and analyzed magnetite and pyroxene/amphibole in a Qtz-Px rock (G91-26) from the island of Akilia. This sample contains 35% quartz, 25% clinopyroxene (hedenbergite), 20% orthopyroxene (ferrosilite), 15% amphibole (grunerite), and 5% magnetite (Nutman et al., 1997). The Mgt/Px-Amph fractionation documented by Dauphas et al. (2004a) is $0.114 \pm 0.041‰/amu$. Rocks from Akilia experience granulite facies metamorphism in the early Archean (~750 °C, Griffin et al., 1980) and were retrogressed under amphibolite facies in the late Archean (Nutman et al., 1997). The measured fractionation is compared with predictions from Polyakov and Mineev (2000) and Polyakov et al. (2007) in Fig. 14b. There is good agreement between the measured fractionation and the prediction,

$$\Delta Fe_{magnetite-hedenbergite} = 0.16241x - 1.3546 \times 10^{-3}x^2 + 0.86777 \times 10^{-6}x^3 \ (‰/amu). \quad (2)$$

Beard and Johnson (2004) did not detect any fractionation between magnetite and silicate minerals (olivine, amphibole, and biotite) in igneous rocks with closure temperatures of ~800 °C. Our study shows that in regionally metamorphosed rocks heated to >550 °C, Fe isotopic fractionation between coexisting minerals can be used as a geothermometer.

6. CONCLUSIONS

BIFs from the ISB with high Fe/Ti ratios have trace element characteristics that are consistent with seawater derivation as described by Bolhar et al. (2004), including high Y/Ho ratios (Fig. 7), positive Eu/Eu* anomalies, positive La/La* anomalies, and concave upward REE patterns (Fig. 8). These rocks also have heavy Fe isotopic compositions relative to surrounding igneous rocks (~+0.4‰/amu, Fig. 9). The most likely interpretation is that this signature was inherited from partial oxidation in a marine setting of Fe emanating from a source similar to modern mid-ocean ridge hydrothermal vents (~−0.15‰/amu; Sharma et al., 2001; Beard et al., 2003a; Severmann et al., 2004). At this stage, Fe isotopes provide no clues on which process may have been responsible for Fe oxidation. In particular, the fractionations associated with heterogeneous oxidation (Tamura et al., 1976) and photo-oxidation (Braterman et al., 1983) still need to be documented.

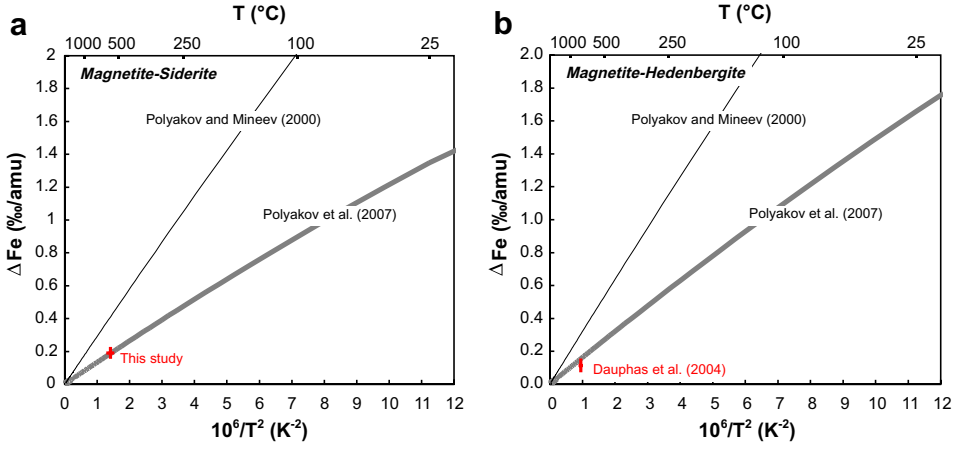

Fig. 14. Comparison between predicted (Polyakov and Mineev, 2000; Polyakov et al., 2007) and measured (Table 5; Dauphas et al., 2004a) Fe isotopic fractionation between magnetite and siderite/hedenbergite. As shown, the new estimates of Polyakov et al. (2007) based on INRXS [Eqs. (1) and (2)] agree with the fractionation measured in sample AL-44 for magnetite–siderite (a, Fig. 6, Section 5.4) and sample G91-26 for magnetite–hedenbergite (b, Dauphas et al., 2004a).

Banded quartz-rich rocks from the island of Akilia with high Fe/Ti ratios share many similarities with *bona fide* BIFs from Isua (heavy Fe isotopic compositions up to +0.4‰/amu, elevated Y/Ho ratios compared to igneous rocks, sometimes positive Eu/Eu^* anomalies) suggesting a chemical sedimentary origin (Figs. 7–9).

The Fe isotope, mineralogical, trace and major element compositions of several bulk metacarbonates were measured. There is a clear distinction between samples with high and low Fe/Ti ratios (Figs. 7 and 8). The Fe-poor metacarbonates from the southwestern part of the belt that were studied by Rose et al. (1996) and Rosing et al. (1996) have light Fe isotopic compositions (~−0.4‰/amu). This is consistent with derivation of these rocks by fluid flow through surrounding igneous rocks and deposition as metasomatic carbonates. The REE patterns and elevated Y/Ho ratios are reminiscent of chemical sediments and it is not clear at present whether metasomatic processes can produce such features.

Iron-rich metacarbonates from the ISB have heavy Fe isotopic compositions relative to IRMM-014 (ranging from 0.1 to 0.4‰/amu) and surrounding igneous rocks (Figs. 9 and 10). Carbonates of sedimentary, hydrothermal, and magmatic origins usually have light Fe isotopic compositions (Fig. 11). The heavy Fe isotopic composition measured in iron-rich metacarbonates from the ISB suggests that Fe in these samples was ultimately derived from ferric-(hydr)oxide produced by partial oxidation of ferrous iron in seawater. The trace element characteristics of the metacarbonates with heavy Fe isotopic compositions and high Fe/Ti ratios are also consistent with the presence of a seawater component (Figs. 7 and 8). The most likely interpretation is that these iron-rich metacarbonates were derived from mobilization of Fe in BIFs by metasomatic fluids.

ACKNOWLEDGMENTS

We thank Alan P. Nutman, Derek Vance, an anonymous reviewer, and Associate Editor Mark Rehkämper for careful and constructive reviews. This study benefited from discussions with V.B. Polyakov, R.N. Clayton, A.M. Davis, N.L. Cates, and S.J. Mojzsis. V.B. Polyakov and R.N. Clayton are thanked for communication of updated β-factors. A.M. Davis provided expertise with SEM analysis at the University of Chicago. I.N. Tolstikhin is thanked for providing the carbonatite samples. This work was supported by the National Aeronautics and Space Administration through grants NNG06GG75G (to N.D.) and NNG05GG22G (to M.W.).

APPENDIX A. SUPPLEMENTARY DATA

Supplementary data associated with this article can be found, in the online version, at doi:10.1016/j.gca.2007.07.019.

REFERENCES

Ague J. J. (1991) Evidence for major mass transfer and volume strain during regional metamorphism of pelites. *Geology* **19**, 855–858.

Alibert C. and McCulloch M. T. (1993) Rare earth element and neodymium isotopic compositions of the banded iron-formations and associated shales from Hamersley, western Australia. *Geochim. Cosmochim. Acta* **57**, 187–204.

Anbar A. D., Jarzecki A. A. and Spiro T. G. (2005) Theoretical investigation of iron isotope fractionation between $Fe(H_2O)$ and $Fe(H_2O)$: implication for iron stable isotope geochemistry. *Geochim. Cosmochim. Acta* **69**, 825–837.

Anders E. and Grevesse N. (1989) Abundances of the elements: meteoritic and solar. *Geochim. Cosmochim. Acta* **53**, 197–214.

André L., Cardinal D., Alleman L. Y. and Moorbath S. (2006) Silicon isotopes in ~3.8 Ga West Greenland rocks as clues to the Eoarchaean supracrustal Si cycle. *Earth Planet. Sci. Lett.* **254**, 162–173.

Appel P. W. U. (1980) On the early Archaean Isua iron formation, West Greenland. *Precambrian Res.* **11**, 73–87.

Appel P. W. U. (1983) Rare earth elements in the early Archaean Isua iron-formation, West Greenland. *Precambrian Res.* **20**, 243–258.

Appel P. W. U., Fedo C. M., Moorbath S. and Myers J. S. (1998) Recognizable primary volcanic and sedimentary features in a low-strain domain of the highly deformed, oldest known (~3.7–3.8 Gyr) Greenstone Belt, Isua, West Greenland. *Terra Nova* **10**, 57–62.

Archer C. and Vance D. (2006) Coupled Fe and S isotope evidence for Archean microbial Fe(III) and sulfate reduction. *Geology* **34**, 153–156.

Balci N., Bullen T. D., Witte-Lien K., Shanks W. C., Motelica M. and Mandernack K. W. (2006) Iron isotope fractionation during microbially stimulated Fe(II) oxidation and Fe(III) precipitation. *Geochim. Cosmochim. Acta* **70**, 622–639.

Bau M. and Möller P. (1993) Rare earth element systematics of the chemically precipitated component in Early Precambrian iron formations and the evolution of the terrestrial atmosphere–hydrosphere–lithosphere system. *Geochim. Cosmochim. Acta* **57**, 2239–2249.

Bau M. (1996) Controls on the fractionation of isovalent trace elements in magmatic and aqueous systems: evidence from Y/Ho Zr/Hf, and lanthanide tetrad effect. *Contrib. Mineral. Petrol.* **123**, 323–333.

Bau M. and Dulski P. (1996) Distribution of yttrium and rare-earth elements in the Penge and Kuruman iron-formations, Transvaal Supergroup, South Africa. *Precambrian Res.* **79**, 37–55.

Bau M. (1999) Scavenging of dissolved yttrium and rare earths by precipitating iron oxyhydroxide: experimental evidence for Ce oxidation Y–Ho fractionation and lanthanide tetrad effect. *Geochim. Cosmochim. Acta* **63**, 67–77.

Beard B. L., Johnson C. M., Cox L., Sun H., Nealson K. H. and Aguilar C. (1999) Iron isotope biosignatures. *Science* **285**, 1889–1892.

Beard B. L., Johnson C. M., von Damm K. L. and Poulson R. L. (2003a) Iron isotope constraints on Fe cycling and mass balance in oxygenated Earth oceans. *Geology* **31**, 629–632.

Beard B. L., Johnson C. M., Skulan J. L., Nealson K. H., Cox L. and Sun H. (2003b) Application of Fe isotopes to tracing the geochemical and biological cycling of Fe. *Chem. Geol.* **195**, 87–117.

Beard B. L. and Johnson C. M. (2004) Inter-mineral Fe isotope variations in mantle-derived rocks and implications for the Fe geochemical cycle. *Geochim. Cosmochim. Acta* **68**, 4727–4743.

Boak J. L. and Dymek R. F. (1982) Metamorphism of the ca. 3800 Ma supracrustal rocks at Isua, West Greenland: implications for early Archaean crustal evolution. *Earth Planet. Sci. Lett.* **59**, 155–176.

Bolhar R., Kamber B. S., Moorbath S., Fedo C. M. and Whitehouse M. J. (2004) Characterisation of early Archaean chemical sediments by trace element signatures. *Earth Planet. Sci. Lett.* **222**, 43–60.

Brantley S. L., Liermann L. and Bullen T. D. (2001) Fractionation of Fe isotopes by soil microbes and organic acids. *Geology* **29**, 535–538.

Brantley S. L., Liermann L. J., Guynn R. L., Anbar A., Icopini G. A. and Barling J. (2004) Fe isotopic fractionation during mineral dissolution with and without bacteria. *Geochim. Cosmochim. Acta* **68**, 3189–3204.

Braterman P. S., Cairns-Smith A. G. and Sloper R. W. (1983) Photo-oxidation of hydrated Fe^{2+}—significance for banded iron formations. *Nature* **303**, 163–164.

Bullen T. D., White A. F., Childs C. W., Vivit D. V. and Schulz M. S. (2001) Demonstration of significant abiotic iron isotope fractionation. *Geology* **29**, 699–702.

Byrne R. H. and Kim K.-H. (1990) Rare earth element scavenging in seawater. *Geochim. Cosmochim. Acta* **54**, 2645–2656.

Byrne R. H. and Lee J. H. (1993) Comparative yttrium and rare earth element chemistries in seawater. *Mar. Chem.* **44**, 121–130.

Cates N. L. and Mojzsis S. J. (2006) Chemical and isotopic evidence for widespread Eoarchean metasedimentary enclaves in southern West Greenland. *Geochim. Cosmochim. Acta* **70**, 4229–4257.

Cates N. L. and Mojzsis S. J. (2007) Pre-3750 Ma supracrustal rocks from the Nuvvuagittuq supracrustal belt, northern Québec. *Earth Planet. Sci. Lett.* **255**, 9–21.

Cloud P. (1983) Banded iron-formation—a gradualist's dilemna. In *Iron-Formation: Formation: Facts and Problems* (eds. A. F. Trendall and R. C. Morris). Elsevier, Amsterdam, pp. 401–416.

Croal L. R., Johnson C. M., Beard B. L. and Newman D. K. (2004) Iron isotope fractionation by Fe(II)-oxidizing photoautotrophic bacteria. *Geochim. Cosmochim. Acta* **68**, 1227–1242.

Crosby H. A., Johnson C. M., Roden E. E. and Beard B. L. (2005) Coupled Fe(II)–Fe(III) electron and atom exchange as a mechanism for Fe isotope fractionation during dissimilatory iron oxide reduction. *Environ. Sci. Technol.* **39**, 6698–6704.

Crosby H. A., Roden E. E., Johnson C. M. and Beard B. L. (2007) The mechanisms of iron isotope fractionation produced during dissimilatory Fe(III) reduction by *Shewanella putrefaciens* and *Geobacter sulfurreducens*. *Geobiology* **5**, 169–189.

Danielson A., Möller P. and Dulski P. (1992) The europium anomalies in banded iron formations and the thermal history of the oceanic crust. *Chem. Geol.* **97**, 89–100.

Dauphas N., van Zuilen M., Wadhwa M., Davis A. M., Marty B. and Janney P. E. (2004a) Clues from Fe isotope variations on the origin of early archean BIFs from Greenland. *Science* **306**, 2077–2080.

Dauphas N., Janney P. E., Mendybaev R. A., Wadhwa M., Richter F. M., Davis A. M., van Zuilen M., Hines R. and Foley C. N. (2004b) Chromatographic separation and multicollection—ICPMS analysis of iron. Investigating mass-dependent and -independent isotope effects. *Anal. Chem.* **76**, 5855–5863.

Dauphas N. and Rouxel O. (2006) Mass spectrometry and natural variations of iron isotopes. *Mass Spectrom. Rev.* **25**, 515–550, Erratum 25, 831–832.

Dauphas N., Cates N. L., Mojzsis S. J. and Busigny V. (2007) Identification of chemical sedimentary protoliths using iron isotopes in the >3750 Ma Nuvvuagittuq supracrustal belt, Canada. *Earth Planet. Sci. Lett.* **254**, 358–376.

David J., Parent M., Stevenson R., Nadeau P. and Godin L. (2002) La sequence supracrustale de Porpoise Cove, region d'Inukjuak: un exemple unique de croûte paléo-archéenne (ca. 3.8 Ga) dans la Province du Supérieur, in L'exploration minérale au Québec, notre savoir, vos découvertes, Ministère des Ressources Naturelles, Québec, DV 2002-10, p. 17.

Derry L. A. and Jacobsen S. B. (1990) The chemical evolution of Precambrian seawater: evidence from REEs in banded iron formations. *Geochim. Cosmochim. Acta* **54**, 2965–2977.

Dideriksen K., Baker J. A. and Stipp S. L. S. (2006) Iron isotopes in natural carbonate minerals determined by MC-ICP-MS with a ^{58}Fe–^{54}Fe double spike. *Geochim. Cosmochim. Acta* **70**, 118–132.

Dimroth E. (1982) The oldest rocks on Earth: stratigraphy and sedimentology of the 3.8 billion years old Isua supracrustal sequence. In *Sedimentary Geology of the Highly Metamorphosed Precambrian Complexes* (ed. A. V. Sidorenko). Nauka, Moscow.

Dymek R. F. and Klein C. (1988) Chemistry, petrology and origin of banded iron-formation lithologies from the 3800 Ma Isua Supracrustal Belt, West Greenland. *Precambrian Res.* **39**, 247–302.

Elderfield H. (1988) The oceanic chemistry of rare-earth elements. *Phil. Trans. R. Soc. Lond. A* **325**, 105–126.

Fedo C. M. (2000) Setting and origin for problematic rocks from the >3.7 Ga Isua Greenstone Belt, southern west Greenland: Earth's oldest coarse clastic sediments. *Precambrian Res.* **101**, 69–78.

Fedo C. M., Myers J. S. and Appel P. W. U. (2001) Depositional setting and paleogeographic implications of Earth's oldest supracrustal rocks, the >3.7 Ga Isua Greenstone belt, West Greenland. *Sediment. Geol.* **141**, 61–77.

Fedo C. M. and Whitehouse M. J. (2002a) Metasomatic origin of quartz-pyroxene rock, Akilia, Greenland and implications for Earth's earliest life. *Science* **296**, 1448–1452.

Fedo C. M. and Whitehouse M. J. (2002b) Origin and significance of Archean quartzose rocks at Akilia, Greenland—response. *Science* **298**, 917a.

Fedo C. M. and Whitehouse M. J. (2002c) The origin of a most contentious rock—response. *Science* **298**, 961–962.

Fedo C. M., Whitehouse M. J. and Kamber B. S. (2006) Geological constraints on detecting the earliest life on Earth: a perspective from the Early Archaean (older than 3.7 Gyr) of southwest Greenland. *Phil. Trans. R. Soc. (Lond.) B* **361**, 851–867.

Frei R., Bridgwater D., Rosing M. and Stecher O. (1999) Controversial Pb–Pb and Sm–Nd isotope results in the early Archaean Isua (west Greenland) oxide iron formation: preservation of primary signatures versus secondary disturbances. *Geochim. Cosmochim. Acta* **63**, 473–488.

Frei R. and Rosing M. T. (2001) The least terrestrial leads; implications for the early Archaean crustal evolution and hydrothermal-metasomatic processes in the Isua supracrustal belt (west Greenland). *Chem. Geol.* **181**, 47–66.

Frei R. and Jensen B. K. (2003) Re–Os, Sm–Nd isotope and REE systematics on ultramafic rocks and pillow basalts from the Earth's oldest oceanic crustal fragments (Isua Supracrustal Belt and Ujaragssuit nunât area, W. Greenland). *Chem. Geol.* **196**, 163–191.

Frei R. and Polat A. (2007) Source heterogeneity for the major components of ~3.7 Ga banded iron formations (Isua Greenstone Belt, Western Greenland): tracing the nature of interacting water masses in BIF formation. *Earth Planet. Sci. Lett.* **253**, 266–281.

Friend C. R. L., Nutman A. P. and Bennett V. C. (2002) Origin and significance of Archean quartzose rocks at Akilia, Greenland—comment. *Science* **298**, 917a.

Frost C. D., von Blanckenburg F., Schoenberg R., Frost B. R. and Swapp S. M. (2007) Preservation of Fe isotope heterogeneities during diagenesis and metamorphism of banded iron formation. *Contrib. Mineral. Petrol.* **153**, 211–235.

Furnes H., de Wit M., Staudigel H., Rosing M. and Muehlenbachs K. (2007) A vestige of Earth's oldest ophiolite. *Science* **315**, 1704–1707.

Govindaraju K. (1994) 1994 compilation of working values and sample description for 383 geostandards. *Geostandard. Newslett.* **18**, 1–158.

Grau G., Rosing M., Bridgwater D. and Gill R. C. O. (1996) Resetting of Sm–Nd systematics during metamorphism of >3.7 Ga rocks: implications for isotopic models of early earth differentiation. *Chem. Geol.* **133**, 225–240.

Griffin W. L., McGregor V. R., Nutman A., Taylor P. N. and Bridgwater D. (1980) Early Archeaean granulite-facies metamorphism south of Ameralik, West Greenland. *Earth Planet. Sci. Lett.* **50**, 59–74.

Icopini G. A., Anbar A. D., Ruebush S. S., Tien M. and Brantley S. L. (2004) Iron isotope fractionation during microbial reduction of iron: the importance of adsorption. *Geology* **32**, 205–208.

Jacobsen S. B. and Pimentel-Klose M. R. (1988) A Nd isotopic study of the Hamersley and Michipicoten banded iron formations: the source of REE and Fe in Archean oceans. *Earth Planet. Sci. Lett.* **87**, 29–44.

Jochum K. P., Seufert H. M., Spettel B. and Pal me H. (1986) The solar system abundances of Nb, Ta, and Y, and the relative abundances of refractory lithophile elements in differentiated planetary bodies. *Geochim. Cosmochim. Acta* **50**, 1173–1183.

Jochum K. P., McDonough W. F., Palme H. and Spettel B. (1989) Compositional constraints on the continental lithospheric mantle from trace elements in spinel peridotite xenoliths. *Nature* **340**, 548–550.

Johnson C. M., Beard B. L., Beukes N. J., Klein C. and O'Leary J. M. (2003) Ancient geochemical cycling in the Earth as inferred from Fe isotope studies of banded iron formations from the Transvaal Craton. *Contrib. Mineral. Petrol.* **144**, 523–547.

Johnson C. M., Roden E. E., Welch S. A. and Beard B. L. (2005) Experimental constraints on Fe isotope fractionation during magnetite and Fe carbonate formation coupled to dissimilatory hydrous ferric oxide reduction. *Geochim. Cosmochim. Acta* **69**, 963–993.

Kasting J. F. (1987) Theoretical constraints on oxygen and carbon dioxide concentrations in the Precambrian atmosphere. *Precambrian Res.* **34**, 205–229.

Komiya T., Maruyama S., Masuda T., Nohda S., Hayashi M. and Okamoto K. (1999) Plate tectonics at 3.8–3.7 Ga: field evidence from the Isua accretionary complex, southern West Greenland. *J. Geol.* **107**, 515–554.

Komiya T., Maruyama S., Hirata T., Yurimoto H. and Nohda S. (2004) Geochemistry of the oldest MORB and OIB in the Isua Supracrustal Belt, southern West Greenland: implications for the composition and temperature of early Archean upper mantle. *The Island Arc* **13**, 47–72.

Lepland A., Arrhenius G. and Cornell D. (2002) Apatite in early Archean Isua supracrustal rocks, southern West Greenland: its origin, association with graphite and potential as a biomarker. *Precambrian Res.* **118**, 221–241.

Lovley D. R. (1991) Dissimilatory Fe(III) and Mn(IV) reduction. *Microbiol. Rev.* **55**, 259–287.

Manning C. E., Mojzsis S. J. and Harrison T. M. (2006) Geology, age and origin of supracrustal rocks at Akilia, West Greenland. *Am. J. Sci.* **306**, 303–366.

Markl G., von Blanckenburg F. and Wagner T. (2006) Iron isotope fractionation during hydrothermal ore deposition and alteration. *Geochim. Cosmochim. Acta* **70**, 3011–3030.

McDonough W. F. and Sun S.-S. (1995) The composition of the Earth. *Chem. Geol.* **120**, 223–253.

McGregor V. R. and Mason B. (1977) Petrogenesis and geochemistry of metabasaltic and metasedimentary enclaves in the Amîtsoq gneisses, West Greenland. *Am. Mineral.* **62**, 887–904.

Mojzsis S. J., Arrhenius G., McKeegan K. D., Harrison T. M., Nutman A. P. and Friend C. R. L. (1996) Evidence for life on Earth before 3800 million years ago. *Nature* **384**, 55–59.

Mojzsis S. J. and Harrison T. M. (2002) Origin and significance of Archean quartzose rocks at Akilia, Greenland—comment. *Science* **298**, 917a.

Mojzsis S. J., Coath C. D., Greenwood J. P., McKeegan K. D. and Harrison T. M. (2003) Mass-independent isotope effects in Archean (2.5 to 3.8 Ga) sedimentary sulfides determined by ion microprobe analysis. *Geochim. Cosmochim. Acta* **67**, 1635–1658.

Moorbath S., O'Nions R. K. and Pankhurst R. J. (1973) Early Archaean age of the Isua iron formation, West Greenland. *Nature* **245**, 138–139.

Myers J. S. and Crowley J. L. (2000) Vestiges of life in the oldest Greenland rocks? A review of early Archaean geology in the Godthaabsfjord region, and reappraisal of field evidence for >3850 Ma life on Akilia. *Precambrian Res.* **103**, 101–124.

Myers J. S. (2001) Protoliths of the 3.8–3.7 Ga Isua greenstone belt, West Greenland. *Precambrian Res.* **105**, 129–141.

Nozaki Y., Zhang Y. S. and Amakawa H. (1997) The fractionation between Y and Ho in the marine environment. *Earth Planet. Sci. Lett.* **148**, 329–340.

Nutman A. P., Allaart J. H., Bridgwater D., Dimroth E. and Rosing M. T. (1984) Stratigraphic and geochemical evidence for the depositional environment of the early Archaean Isua supracrustal belt, southern West Greenland. *Precambrian Res.* **25**, 365–396.

Nutman A. P. (1986) The early Archaean to Proterozoic history of the Isuakasia area, southern West Greenland. *Geol. Survey Greenland Bull.*, 154.

Nutman A. P., Fryer B. and Bridgwater D. (1989) The early Archaean Nulliak (supracrustal) assemblage, northern Labrador. *Can. J. Earth Sci.* **26**, 2159–2168.

Nutman A. P., McGregor V. R., Friend C. R. L., Bennett V. C. and Kinny P. D. (1996) The Itsaq Gneiss Complex of southern West Greenland; the world's most extensive record of early crustal evolution (3900–3600 Ma). *Precambrian Res.* **78**, 1–39.

Nutman A. P., Mojzsis S. J. and Friend C. R. L. (1997) Recognition of ⩾3850 Ma water-lain sediments in West Greenland and their significance for the early Archaean Earth. *Geochim. Cosmochim. Acta* **61**, 2475–2484.

Nutman A. P., Friend C. R. L., Bennett V. C. and McGregor V. R. (2000) The early Archaean Itsaq Gneiss Complex of southern West Greenland: the importance of field observations in interpreting age and isotopic constraints for early terrestrial evolution. *Geochim. Cosmochim. Acta* **64**, 3035–3060.

Nutman A. P., Friend C. R. L. and Bennett V. C. (2002a) Evidence for 3650–3600 Ma assembly of the northern end of the Itsaq Gneiss Complex, Greenland: implication for early Archaean tectonics. *Tectonics* **21**. doi:10.1029/2000TC001203.

Nutman A. P., McGregor V. R., Shiraishi K., Friend C. R. L., Bennett V. C. and Kinny P. D. (2002b) >3850 Ma BIF and mafic inclusions in the early Archaean Itsaq Gneiss Complex around Akilia, southern West Greenland? The difficulties of precise dating of zircon-free protoliths in migmatites. *Precambrian Res.* **117**, 185–224.

Nutman A. P. and Friend C. R. L. (2006) Petrography and geochemistry of apatites in banded iron formation, Akilia, W. Greenland: consequences for oldest life evidence. *Precambrian Res.* **147**, 100–106.

O'Hara K. and Blackburn W. H. (1989) Volume-loss model for trace-element enrichments in mylonites. *Geology* **17**, 524–527.

Ohmoto H., Watanabe Y. and Kumazawa K. (2004) Evidence from massive siderite beds for a CO_2-rich atmosphere before ~1.8 billion years ago. *Nature* **429**, 395–399.

Owen T., Cess R. D. and Ramanathan V. (1979) Enhanced CO_2 greenhouse to compensate for reduced solar luminosity on early Earth. *Nature* **277**, 640–642.

Pack A., Russell S. S., Shelley J. M. G. and van Zuilen M. (2007) Geo- and cosmochemistry of the twin elements yttrium and holmium. *Geochim. Cosmochim. Acta.* **71**, 4592–4608.

Palin J. M. (2002) The origin of a most contentious rock—comment. *Science* **298**, 961.

Perry E. C. and Ahmad S. N. (1977) Carbon isotope composition of graphite and carbonate minerals from 3.8−AE metamorphosed sediments, Isukasia, Greenland. *Earth Planet. Sci. Lett.* **36**, 280–284.

Piepgras D. J., Wasserburg G. J. and Dasch E. J. (1979) The isotopic composition of Nd in different ocean masses. *Earth Planet. Sci. Lett.* **45**, 223–236.

Polat A., Hofmann A. W. and Rosing M. T. (2002) Boninite-like volcanic rocks in the 3.7–3.8 Ga Isua greenstone belt, West Greenland: geochemical evidence for intra-oceanic subduction zone processes in the early Earth. *Chem. Geol.* **184**, 231–254.

Polat A. and Hofmann A. W. (2003) Alteration and geochemical patterns in the 3.7–3.8 Ga Isua greenstone belt, West Greenland. *Precambrian Res.* **126**, 197–218.

Polyakov V. B. and Mineev S. D. (2000) The use of Mössbauer spectroscopy in stable isotope geochemistry. *Geochim. Cosmochim. Acta* **64**, 849–865.

Polyakov V. B., Clayton R. N., Horita J. and Mineev S. D. (2007) Equilibrium iron isotope fractionation factors of minerals: Reevaluation from the data of nuclear inelastic resonant X-ray scattering and Mössbauer spectroscopy. *Geochim. Cosmochim. Acta.* **71**, 3833–3846.

Quinn K. A., Byrne R. H. and Schijf J. (2004) Comparative scavenging of Yttrium and the rare earth elements in seawater: competitive influences of solution and surface chemistry. *Aquat. Geochem.* **10**, 59–80.

Rollinson H. (2002) The metamorphic history of the Isua Greenstone Belt, West Greenland. In *The Early Earth: Physical, Chemical and Biological Development* (eds. C. M. R. Fowler, C. J. Ebinger and C. J. Hawkesworth). Geological Society, Special Publications, London, 199, pp. 329–350.

Rollinson H. (2003) Garnet growth chronologies indicate a complex metamorphic history for the Isua Greenstone Belt. *Precambrian Res.* **126**, 181–196.

Rose N. M., Rosing M. T. and Bridgwater D. (1996) The origin of metacarbonate rocks in the Archean Isua Supracrustal Belt, West Greenland. *Am. J. Sci.* **296**, 1004–1044.

Rosing M. T., Rose N. M., Bridgwater D. and Thomsen H. S. (1996) Earliest part of Earth's stratigraphic record: a reappraisal of the >3.7 Ga Isua (Greenland) supracrustal sequence. *Geology* **24**, 43–46.

Rosing M. T. (1999) ^{13}C-Depleted carbon microparticles in >3700-Ma sea-floor sedimentary rocks from West Greenland. *Science* **283**, 674–676.

Rouxel O., Dobbek N., Ludden J. and Fouquet Y. (2003) Iron isotope fractionation during oceanic crust alteration. *Chem. Geol.* **202**, 155–182.

Rouxel O. J., Bekker A. and Edwards K. (2005) Iron isotope constraints on the Archean and Paleoproterozoic ocean redox state. *Science* **307**, 1088–1091.

Rouxel O. J., Bekker A. and Edwards K. J. (2006) Response to comment on Iron isotope constraints on the Archean and Paleoproterozoic ocean redox state. *Science* **311**, 177b.

Rye R., Kuo P. H. and Holland H. D. (1995) Atmospheric carbon dioxide concentrations before 2.2 billion years ago. *Nature* **378**, 603–605.

Schidlowski M., Appel P. W. U., Eichmann R. and Junge C. E. (1979) Carbon isotope geochemistry of the 3.7 × 109-yr-old Isua sediments, West Greenland: implications for the Archaean carbon and oxygen cycles. *Geochim. Cosmochim. Acta* **43**, 189–199.

Schiøtte L., Compston W. and Bridgwater D. (1989) U–Th–Pb ages of single zircons in Archaean supracrustals from the Nain Province, Labrador, Canada. *Can. J. Earth Sci.* **26**, 2636–2644.

Severmann S., Johnson C. M., Beard B. L., German C. R., Edmonds H. N., Chiba H. and Green D. R. H. (2004) The effect of plume processes on the Fe isotope composition of hydrothermally derived Fe in the deep ocean as inferred from the Rainbow vent site, Mid-Atlantic Ridge, 36°14′N. *Earth Planet. Sci. Lett.* **225**, 63–76.

Severmann S., Johnson C. M., Beard B. L. and McManus J. (2006) The effect of early diagenesis on the Fe isotope compositions of porewaters and authigenic minerals in continental margin sediments. *Geochim. Cosmochim. Acta* **70**, 2006–2022.

Sharma M., Polizzotto M. and Anbar A. D. (2001) Iron isotopes in hot springs along the Juan de Fuca Ridge. *Earth Planet. Sci. Lett.* **194**, 39–51.

Shimizu H., Umemoto N., Masuda A. and Appel P. W. U. (1990) Sources of iron-formation in the Archean Isua and Malene supracrustals, West Greenland: evidence from La–Ce and Sm–Nd isotopic data and REE abundances. *Geochim. Cosmochim. Acta* **54**, 1147–1154.

Skulan J. L., Beard B. L. and Johnson C. M. (2002) Kinetic and equilibrium Fe isotope fractionation between aqueous Fe(III) and hematite. *Geochim. Cosmochim. Acta* **66**, 2995–3015.

Staubwasser M., von Blanckenburg F. and Schoenberg R. (2006) Iron isotopes in the early marine diagenetic iron cycle. *Geology* **34**, 629–632.

Tamura H., Goto K. and Nagayama M. (1976) The effect of ferric hydroxide on the oxygenation of ferrous ions in neutral solutions. *Corros. Sci.* **16**, 197–207.

Taylor P. D. P., Maeck R. and De Bièvre P. (1992) Determination of the absolute isotopic composition and atomic weight of a reference sample of natural iron. *Int. J. Mass Spectrom. Ion Process.* **121**, 111–125.

van Zuilen M. A., Lepland A. and Arrhenius G. (2002) Reassessing the evidence for the earliest traces of life. *Nature* **418**, 627–630.

van Zuilen M. A., Lepland A., Teranes J., Finarelli J., Wahlen M. and Arrhenius G. (2003) Graphite and carbonates in the 3.8 Ga old Isua Supracrustal Belt, southern West Greenland. *Precambrian Res.* **126**, 331–348.

van Zuilen M. A., Mathew K., Wopenka B., Lepland A., Marti K. and Arrhenius A. (2005) Nitrogen and argon isotopic signatures in graphite from the 3.8-Ga-old Isua Supracrustal Belt, southern West Greenland. *Geochim. Cosmochim. Acta* **69**, 1241–1252.

Welch S. A., Beard B. L., Johnson C. M. and Braterman P. S. (2003) Kinetic and equilibrium Fe isotope fractionation between aqueous Fe(II) and Fe(III). *Geochim. Cosmochim. Acta* **67**, 4231–4250.

Whitehouse M. J., Kamber B. S. and Moorbath S. (1999) Age significance of U–Th–Pb zircon data from early Archaean rocks of west Greenland—a reassessment based on combined ion-microprobe and imaging studies. *Chem. Geol.* **160**, 201–224.

Whitehouse M. J., Kamber B. S., Fedo C. M. and Lepland A. (2005) Integrated Pb- and S-isotope investigation of sulphide minerals from the early Archaean of southwest Greenland. *Chem. Geol.* **222**, 112–131.

Widdel F., Schnell S., Heising S., Ehrenreich A., Assmus B. and Schink B. (1993) Ferrous iron oxidation by anoxygenic phototrophic bacteria. *Nature* **362**, 834–836.

Yamaguchi K. E. and Ohmoto H. (2006) Comment on Iron isotope constraints on the Archean and Paleoproterozoic ocean redox state. *Science* **311**, 177a.

Zhang J., Amakawa H. and Nozaki Y. (1994) The comparative behaviors of Yttrium and Lanthanides in the seawater of the North Pacific. *Geophys. Res. Lett.* **21**, 2677–2680.

Associate editor: Mark Rehkamper